

The giant Ruatoria debris avalanche on the northern Hikurangi margin, New Zealand: Result of oblique seamount subduction

Jean-Yves Collot

UMR Géosciences Azur, Institut de Recherche pour le Développement, Villefranche sur mer, France

Keith Lewis and Geoffroy Lamarche

National Institute of Water and Atmospheric Research, Wellington, New-Zealand

Serge Lallemand

Laboratoire de Géophysique, Tectonique et Sédimentologie, Université de Montpellier II, Montpellier, France

Abstract. Despite convergent margins being unstable systems, most reports of huge submarine slope failure have come from oceanic volcanoes and passive margins. Swath bathymetry and seismic profiles of the northern Hikurangi subduction system, New Zealand, show a tapering 65–30 km wide by 65 km deep margin indentation, with a giant, $3150 \pm 630 \text{ km}^3$, blocky, debris avalanche deposit projecting 40 km out across horizontal trench fill, and a debris flow deposit projecting over 100 km. Slide blocks are well-bedded, up to 18 km across and 1.2 km high, the largest being at the avalanche deposit's leading edge. Samples dredged from them are mainly Miocene shelf calc-mudstones similar to those outcropping around the indentation. Cores from cover beds suggest that failure occurred $\sim 170 \pm 40 \text{ ka}$, possibly synchronously with a major extension collapse in the upper indentation. However, the northern part of the indentation is much older. The steep, straight northern wall is close to the direction of plate convergence and probably formed around 2.0–0.16 Ma as a large seamount subducted, leaving in its wake a deep groove obliquely across the margin and an unstable triangle of fractured rock in the 60° angle between groove and oversteepened margin front. The triangle collapsed as a blocky avalanche, leaving a scalloped southern wall and probably causing a large tsunami. Tentative calculations of compacted volumes suggest that the indentation is over 600 km^3 larger than the avalanche, supporting a two-stage origin that includes subduction erosion. Since failure, convergence has carried the deposits $\sim 9 \text{ km}$ back toward the margin, causing internal compression. The eventual subduction/accretion of the Ruatoria avalanche explains the scarcity of such features on active margins and perhaps the nature of olistostromes in fold belts.

1. Introduction

Submarine avalanches and debris flows can be enormous. Those that occur on slopes between land and deep ocean basins can be several orders of magnitude larger than the largest landslides onshore [Hampton *et al.*, 1996]. They can involve the catastrophic movement of hundreds or even thousands of cubic kilometers of broken rock and sediment. They are a threat to offshore structures, such as cables and platforms, and they can devastate coastal areas both by onshore retrogression at their head [Coulter and Migliaccio, 1966; Mulder and Cochonat, 1996] and by generation of large tsunamis [Bondevik *et al.*, 1997; Moore and Moore, 1984]. Ancient masses of broken blocks have been described as “chaos deposits”, melanges or olistostromes in fold belts around the world [Abbate *et al.*, 1970; Ballance and Sporli, 1979; Hsu, 1974; Naylor, 1981; Orange and Underwood, 1995], with debate often centering on whether particular deposits are gravitational or tectonic in origin.

Large submarine slope failure occurs in a variety of forms that can be categorized by what can be regarded as end-members of a continuum of gravitational processes. Perhaps the largest submarine landslides are rotational slumps that involve the slow or intermittent, downslope movement of largely intact, back-tilting blocks on glide planes as much as 10 km below the seabed [Moore and Normark, 1994]. On the other hand, large catastrophic slope failure occurs as disaggregated debris avalanches, with blocks up to many kilometers across and run-out distances of many tens to more than a hundred kilometers [Bugge *et al.*, 1987; Moore *et al.*, 1989; Moore and Normark, 1994]. Similar, but generally smaller, thinner, and more disaggregated sediment slurries, with fewer and rafted blocks, are generally referred to as debris flows [Enos, 1977; Masson *et al.*, 1998]. They travel further than debris avalanches, perhaps because they travel faster in the same environment [Jacobs, 1995; Weaver, 1995], and part of them may incorporate water and mud to metamorphose into turbidity currents capable of travelling a thousand kilometers or more [Garcia and Hull, 1994].

Massive margin failure can occur in a variety of geologic settings. Perhaps the best documented are on the flanks of oceanic “hot spot” volcanoes, where quenching of lava has

Copyright 2001 by the American Geophysical Union.

Paper number 2001JB900004.
0148-0227/01/2001JB900004\$09.00

critically oversteepened slopes [Holcomb and Searle, 1991]. At Hawaiian Islands [Jacobs, 1995; Moore et al., 1989; Moore and Normark, 1994], Canary Islands [Masson, 1996; Masson et al., 1998; Urgeles et al., 1997] and Fournaise volcano near Reunion Island [Lenat et al., 1989], it has been shown that enormous rotational slumps, debris avalanches, and debris flows, some thousand of cubic kilometers in volume and extending above sea level, have collapsed catastrophically into the surrounding deep ocean basin.

Passive margins are also the location of large submarine slope failure. In some cases, failure is associated with excess pore pressure in sedimentary rocks being maintained by gas, often from unstable clathrates [Bugge et al., 1987; Carpenter, 1981; Lerche and Bagirov, 1998]. In other cases, failure results from rapid sediment overloading or tectonic stresses resulting from, among other things, isostatic rebound [Bugge et al., 1987]. Notable examples occur off Norway [Bugge et al., 1987; Jansen, 1987], South Africa [Dingle, 1980], and Northwest Africa [Masson et al., 1998; Weaver, 1995].

Many of the same causes of instability occur at convergent margins, where active forearc slopes are maintained at a critical angle, suggesting that they should be a privileged location for catastrophic slope failure. Continental collision zones such as the Gibraltar Arc are the location of giant, submarine, chaotic bodies [Torelli et al., 1997]. Moderate- to large-sized landslides have been reported from the Sunda Arc

[Moore et al., 1976], the Aleutian Trench [Lewis et al., 1988], Peru [Bourgois et al., 1993; Duperret et al., 1995; von Huene et al., 1989], Costa Rica [Hinz, 1996], and Japan [Cadet et al., 1987]. Subduction of oceanic asperities, commonly seamounts, have produced indentations in convergent margins around the world, with only small landslides in their wake [Lallemant et al., 1990].

In this paper, we document the massive Ruatoria debris avalanche and debris flow associated with a large-scale, morphologic indentation of the Hikurangi subduction margin east of North Island, New Zealand. We interpret the indentation and slope failure association from geophysical data to suggest that they result primarily from the Quaternary subduction of a large seamount. We then focus on the dynamics of avalanching and mass balance calculations, infer that oblique seamount impact encourages larger margin collapse compared with orthogonal convergence, and finally discuss the apparent scarcity of such features on active margins.

2. Geological Setting of Ruatoria Indentation and Avalanche

The Ruatoria indentation and avalanche are located at the northern extremity of the Hikurangi margin, offshore from East Cape (Figure 1). The Hikurangi margin is at the southern

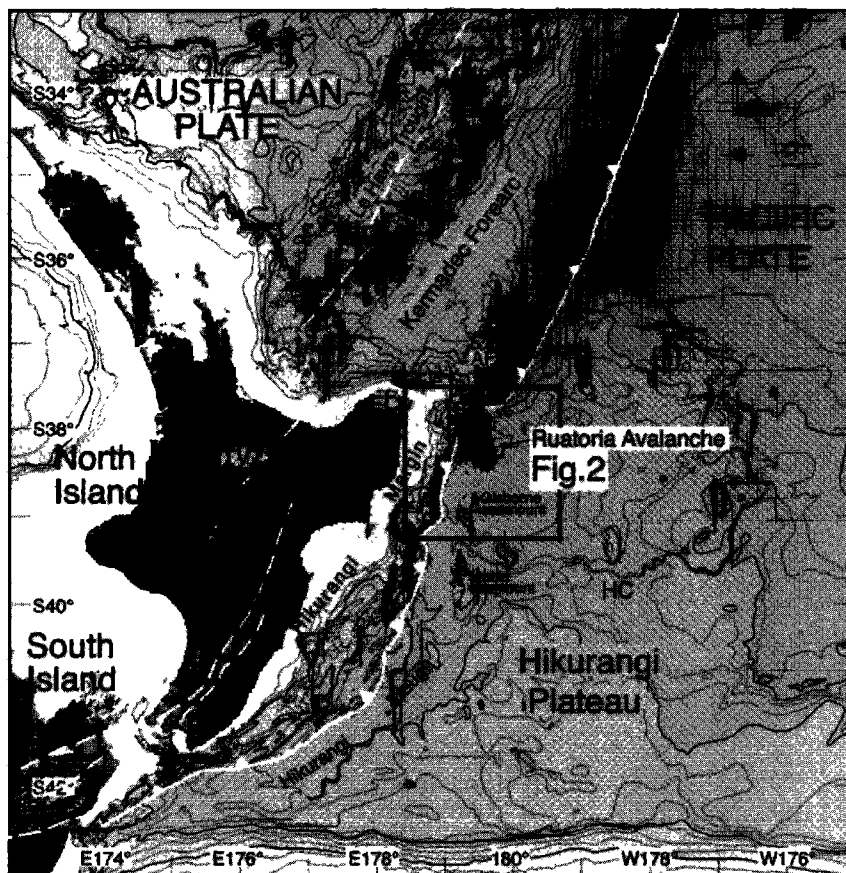


Figure 1. Location of the Ruatoria avalanche and margin indentation. Flagged line is the convergent plate boundary between subducting Pacific Plate and the edge of the Australian Plate east of the back arc Havre Trough and Taupo Volcanic Zone (TVZ), referred to as the Kermadec Forearc. The Hikurangi Plateau is thickened, seamount-studded oceanic crust being subducted at the sediment-starved southern Kermadec Trench and sediment-filled Hikurangi Trough. EC is East Cape. HC is the Hikurangi Channel. AF is Awanui Fault.

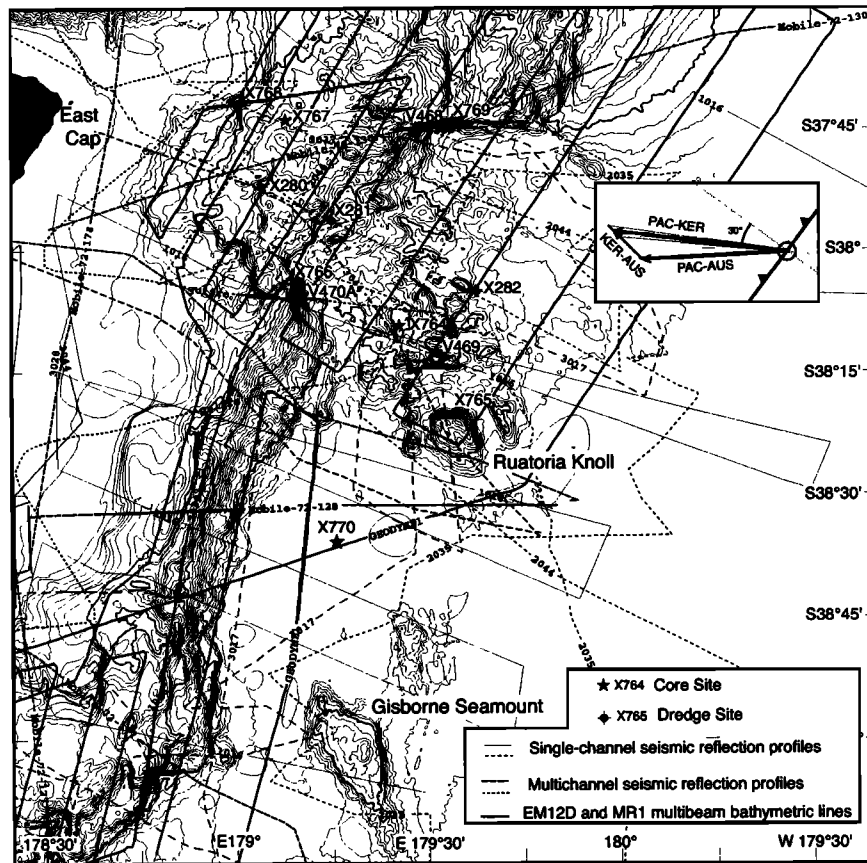


Figure 2. Geophysical lines, rock samples and cores used in this study. Bathymetry is at 100-m intervals. Inset shows convergence vectors between Pacific Plate (PAC), Australian Plate (AUS), and Kermadec Forearc (KER) relative to the deformation front (flagged line). KER-AUS vector was estimated from back arc kinematics. Back arc extension rates decrease from 15–20 mm yr⁻¹ in the southern Havre Trough [Wright, 1993] to 8–12 mm yr⁻¹ in the Taupo Volcanic Zone, on the basis of onshore geodetic triangulations [Walcott, 1987] and integration of GPS measurements [Darby and Meertens, 1995]. The direction of extension ranges from N124°E ± 13 to N135°E, on the basis of GPS data [Darby and Meertens, 1995] and earthquake T axis azimuths [Anderson et al., 1990; Pelletier and Louat, 1989]. Averaging these values, we estimate a rate of back arc opening (KER-AUS) of 12.5 mm yr⁻¹ in a direction N135°E for the latitude of the Ruatoria indentation. Using these values, the PAC-KER convergence is 54 mm yr⁻¹ in a direction N277°E.

end of the Tonga-Kermadec-Hikurangi subduction system, where convergence between the Pacific Plate (PAC) and the overriding Australian Plate (AUS) decreases and becomes progressively more oblique toward the south. The relative PAC-AUS plate motion at the northern extremity of the Hikurangi margin is 45 mm yr⁻¹ in a direction of 267°E [De Mets et al., 1994]. Considering back arc opening in the Taupo Volcanic Zone and Havre Trough, the speed of convergence between Pacific Plate and the Kermadec Forearc (KER) (Figure 1), including the northern Hikurangi margin, is 54 mm yr⁻¹ in a direction N277°E (PAC-KER in Figure 2).

Along the Hikurangi margin, the oceanic Hikurangi Plateau on the Pacific Plate is subducted beneath thinning continental crust on the feather edge of the Australian Plate [Lewis and Pettinga, 1993; Walcott, 1978]. The Hikurangi Plateau is up to ~600 km wide and is believed to be 12–15 km thick Cretaceous oceanic crust [Davy, 1992; Mortimer and Parkinson, 1996; Wood and Davy, 1994]. The northern part of the plateau is heavily studded with volcanic edifices of probable Cretaceous age [Strong, 1994], although there is tentative evidence to the south of late Miocene or younger seamounts [Lewis and Bennett, 1985]. Many of the large

volcanic seamounts (over 1 km high) and smaller knolls are elongated or aligned in ridges trending N150°E ± 20° [Collot et al., 1996]. Between the seamounts and ridges, the plateau is blanketed by pelagic sediments, < 1 km thick, of mainly late Cretaceous and Paleogene age [Wood and Davy, 1994], which also underlie the subduction trench, both in the sediment-flooded Hikurangi Trough and in the sediment-starved southern Kermadec Trench to the north [Lewis et al., 1998]. Within ~200 km of the Hikurangi deformation front, the pelagic layer is covered by a wedge of sheet turbidites originating from a channel system (Figure 1) that turns out of the Hikurangi Trough across the central Hikurangi Plateau [Lewis, 1994].

The Hikurangi margin changes radically from north to south [Lewis and Pettinga, 1993] (Figure 1). Its wide central segment has a foundation of imbricated Cretaceous to upper Miocene shelf slope strata fronted by a 70-km-wide, gently (2°) sloping accretionary prism [Davey et al., 1986; Lewis and Pettinga, 1993], which grew 50 km seaward within the last 0.5 Myr [Barnes and Mercier de Lépinay, 1997]. In contrast, the narrow northern segment lacks a recent accretionary wedge and its frontal part is steep (10°). It is the site of tectonic erosion by a seamount-studded subducting plate with limited sediment

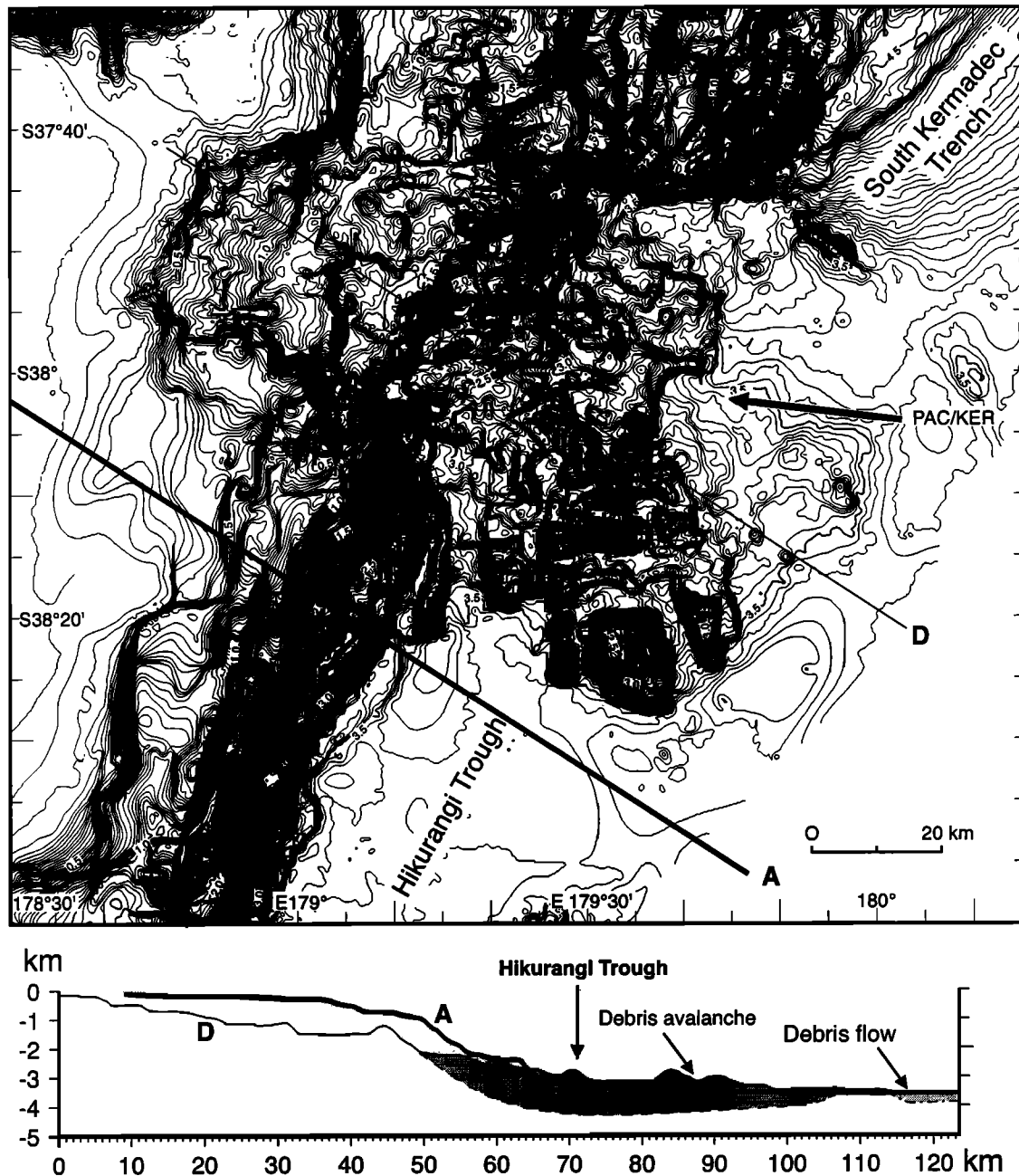


Figure 3. (top) Bathymetry of the Ruatoria avalanche and associated margin indentation with contours at 25-m intervals. (bottom) Bathymetric cross sections A and D across the margin with base of avalanche shown by dashed line. Cross sections are located on bathymetric map.

cover, the deformation front being offset landward by 10-25 km compared with the margins to north and south [Collot *et al.*, 1996; Davey *et al.*, 1997]. Onshore, the northern margin's foundation of Cretaceous-Paleogene rocks is overthrust by the vast East Coast Allochthon or nappe obducted from the NE during early Miocene time [Rait, 1995; Stoneley, 1968]. The allochthon is overlain by Neogene and Quaternary shelf slope sediments, and the whole series has been involved in upper Cainozoic compressional tectonics [Field *et al.*, 1997].

Immediately north of the Ruatoria indentation, the Hikurangi Plateau is subducting beneath the oceanic Kermadec Ridge. The southern Kermadec margin consists of a

nongrowing oversteepened accretionary wedge, dissected by transcurrent faults and tectonically eroded by the subducting Hikurangi Plateau [Collot and Davy, 1998]. This wedge is separated from the more stable, upper part of the margin, by the 220-km-long, transcurrent, Awanui Fault, which is cut at its southern end by the Ruatoria indentation (Figure 1).

The Ruatoria avalanche was first tentatively recognized from conventional bathymetry by [Lewis and Pettinga, 1993]. The preliminary results of the first swath mapping survey of the area appeared to validate the suggestion that rugged topography in the northern Hikurangi Trough was a product of massive slope failure on the adjacent margin. However, it further prompted a suggestion that the geometry of the

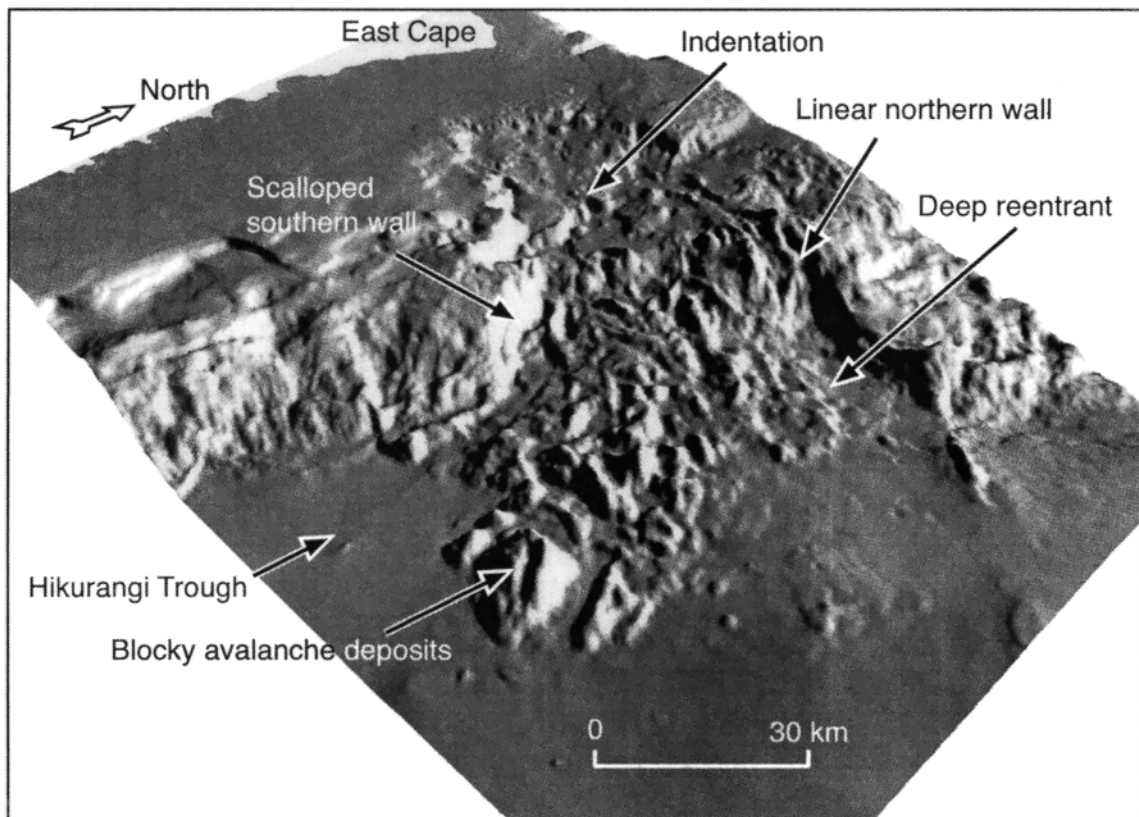


Figure 4. Oblique terrain model of Ruatoria avalanche and indentation showing the linear northern wall, with the deep reentrant in the lower margin, and the scalloped southern wall, with the avalanche deposit at its seaward end. The model also contrasts the block-free upper indentation with the avalanche-covered lower indentation and Hikurangi Trough.

indentation associated with the slope failure deposit indicates not just gravitational effects but also the tectonic effects of seamount subduction [Collot *et al.*, 1996]. This paper describes both indentation and slope failure deposits in much greater detail using a more comprehensive data set and provides new evidence and new interpretations on their nature, age, evolution, and relationship to one another.

3. Geophysical and Geological Data Collection and Processing

Multibeam swath bathymetry and backscatter imagery were recorded across the Ruatoria avalanche deposit and lower part of the indentation during the GeodyNZ cruise of the R/V *L'Atalante*, November 1993 [Collot *et al.*, 1996]. The *L'Atalante's* swath bathymetry and imagery were supplemented with HAWAII MR1 swath data (Figure 2), collected in September 1994 from the New Zealand vessel *Giljanes*. The new swath data were integrated with archived bathymetric data to produce a new bathymetry grid that could be contoured at 25-m intervals, revealing the detailed morphology of the entire indentation and avalanche area (Figures 3 and 4).

Seismic reflection profiles aligned parallel with the margin were obtained during the GeodyNZ cruise. The equipment consisted of two 75 cubic inch GI air guns operating in harmonic mode and a six-channel seismic streamer. Seismic lines transverse to the margin were collected from the R/V *Tangaroa* in March 1998 with a 75-75 cubic inch GI air gun used in harmonic mode and a 24-channel hydrophone array.

Seismic reflection data were processed using Globe Claritas™ seismic processing software to fully migrated sections. Processing included time-domain filtering, predictive deconvolution, threefold stack, and 1500 m s⁻¹ velocity migration. We also reinterpreted a series of seismic reflection profiles archived at National Institute of Water and Atmospheric Research Ltd (NIWA).

In April 1991, April 1995 and May 1999, rocks were dredged from the indentation walls and from slope toe blocks (Figure 2 and Table 1) in an effort to determine the relationship between them. Most of the rock sample resembles Cainozoic mudstones on the adjacent land in appearance and degree of induration. Their age and paleoenvironment were deduced by Stratigraphic Solutions Ltd. from their nannofossil and, in some cases, their foraminiferal content. In May 1999, three cores were obtained from cover beds to try to estimate the age of the indentation and avalanche (Figure 2 and Table 2). Well-defined correlatable tephras in two of the cores were identified by Auckland UniServices Ltd. using electron microprobe glass shard analysis used to calculate sedimentation rates.

4. Morphostructure of Ruatoria Indentation

4.1. Dimensions and Morphological Divisions of the Ruatoria Indentation

The new bathymetric map and Three-dimensional (3-D) diagram of the northern Hikurangi margin (Figures 3 and 4) show a large indentation incising a steep continental slope for

Table 1. Rock Samples From Ruatoria Indentation and Avalanche^a

Station	Latitude	Longitude	Position	Depth, m	Lithology	Age	Paleoenvironment
V469	-38°13'	179°32'	avalanche	2600	calc-mudst	e Pliocene	l shelf - u slope
V470	-38°06'	179°09'	east southern wall	1540	calc-mudst	e-m Miocene	u-m slope
X280	-37°52'	179°04'	top reentrant	1470	calc-mudst	m Miocene	slope
X281	-37°56'	179°15'	head scarp	2200	limest	l Pliocene	slope
X282	-37°05'	179°37'	avalanche	3330	calc-mudst	m Miocene	shelf - u slope
X765a	-38°20'	179°35'	Ruatoria Knoll	~2500	limest	m Oligocene	u slope
X765b	-38°20'	179°35'	Ruatoria Knoll	~2200	calc-mudst	e-m Miocene ?	shelf - u slope
X765c	-38°20'	179°35'	Ruatoria Knoll	~2200	calc-clayst	e Miocene	u - m slope
X765d	-38°20'	179°35'	Ruatoria Knoll	~2200	calc-siltst	e Miocene	shelf - u slope
X766a	-38°05'	179°10'	east southern wall	1700?	calc-mudst	e Miocene ?- e Pliocene	shelf
X766a	-38°05'	179°10'	east southern wall	1700?	calc-mudst	e - m Miocene	shelf
X768	-37°41'	179°01'	west northern wall	936	calc-mudst	l Miocene - e Pliocene	m slope
X769	-37°45'	179°34'	east northern wall	2260	calc-mudst	e Pleistocene	l shelf - u slope

^aLithology abbreviations are mudst, mudstone; limest, limestone; clayst, claystone; siltst, siltstone. Ages are based on nanofossils (e, early; m, mid; l, late). Paleoenvironment is based on nanofossils, foraminifera, and lithology. (l, lower; u, upper).

~65 km landward of a line joining the deformation front on either side (Figure 3). The width of the indentation decreases landward from ~65 km along the interpolated deformation front to ~30 km at the continental shelf. The top of the indentation incises the 140-m contour, and its base is the 3600-m-deep floor of the Hikurangi Trough. The indentation is bound on three sides by steep walls enclosing an area of ~3300 km² (Table 3). On the basis of bathymetric and seismic reflection data we divided the indentation in two structurally distinct parts, a very hummocky lower part, separated by a seaward concave, midslope scarp from a more undulating upper part. In sections 4.2-4.4, we describe a relatively straight northern wall and a highly irregular southern wall, which we consider to be critical to understanding the formation of both the Ruatoria indentation and avalanche. We then show in sections 4.5-4.6 that the upper part of the indentation consists of subsiding sedimentary basins contrasting with its lower part that contains part of the ~3400 km² blocky avalanche (Table 3).

4.2. Straight but Saw-Toothed Northern Wall

The northern wall is 80 km long. Its overall trend is N276°E within 1° of our estimated PAC-KER convergence direction. The wall height ranges from nearly 1400 m on the lower slope to < 200 m on parts of the upper slope, the

steepest parts being inclined at ~22°. Rocks from both ends of the wall are calcareous or tuffaceous mudstone of lower Miocene to lower Pleistocene age (Table 1). The northern wall is divided into eight 5–10 km long segments, which appear dextrally offset by ~1 km, making the wall saw-toothed in plan (Figure 5). Seismic reflection profile GNZ-05 (Figure 6) suggests that on the lower slope, wall segments merge at depth into steeply south dipping faults that may bottom out on the décollement. All of the steeply dipping fault segments of the northern wall together form a linear dextral strike-slip fault system that cuts transversally across the margin (Figure 5). The northern wall on the upper slope is associated with clear normal faulting as discussed later in section 4.5 (Figure 7).

4.3. Irregular, Scalloped, Southern Wall

Compared with the northern wall, the southern wall is irregular and is extensively scalloped in plan view (Figures 3, 4 and 5). On the lower slope its overall trend is ~N320°E, which is significantly different from any value for plate convergence. On the upper slope it trends N280°E, which is within a few degrees of the estimate PAC-KER convergence, and suggests a genetic link with the northern wall. Conspicuous features of this wall are two large arcuate scarps on the lower slope as well as smaller ones on the upper slope.

Table 2. Cores From Ruatoria Indentation, an Enclosed Avalanche Basin, and the Hikurangi Trough Above the Debris Flow Deposit^a

Station	Latitude	Longitude	Position	Depth, m	Length, m	Core log
X764	-38°09'	179°26'	avalanche	3095	2.93	Hemipelagic mud, few silt layers, ashes 54-57 cm Taupo tephra (1.8 ka) 98-100 cm contains peralkaline tephra 109-113 cm Waimihia tephra (3.3 ka) 205-207 cm redeposited 14.7 ka ash 244-247 cm redeposited 14.7 ka ash
X767	-37°44'	179°08'	top reentrant	1302	3.81	hemipelagic mud, few fine-graded silts
X770	-38°36'	179°15'	Hikurangi Trough	3551	0.97	silt turbidites, hemipelagic mud and ashes 61-64 cm Taupo tephra (1.8 ka) 94-97 cm Waimihia tephra (3.3 ka)

^aAsh identifications are based on electron microprobe analysis of glass shards.

Table 3. Areas and Volumes Calculated for the Ruatoria Avalanche, Indentation and Debris Flow^a

Location	Name	Area, km ²	Volume, km ³	Error, 20%, km ³	Por, %	Compacted Volume, km ³	Error, 20%, km ³
Upper indentation	V1	1682	929	186	15	790	158
Lower indentation							
Material loss	V2	1162	579	116	15	492	98
Remains in margin	V3		1515	302	15	1287	257
Material gain	V4		86				
	V2+V3	1612	2094	419	15	1780	356
Total indentation	V1+V2+V3	3295	3023	605	15	2570	514
Total avalanche	Va	3409	3146	629	37.8	1958	392
Difference: (V1+V2+V3)-Va						612	
Debris flow	Vd	8000	960	192	60	384	77

^aUpper and lower indentations are defined in Plate 1d. Numbers are rounded up to closest integer. Por, porosity [Field et al., 1997]; volumes V1, V2, V3, V4 and Va are defined in Plate 1. Volume V3 and Va are calculated with P wave velocity of 2000 m s⁻¹. Compacted volumes, Vol *(100-Por) / 100. Avalanche (Va) compacted volume is calculated in Table 4. Vd is calculated for an average thickness of 120 m.

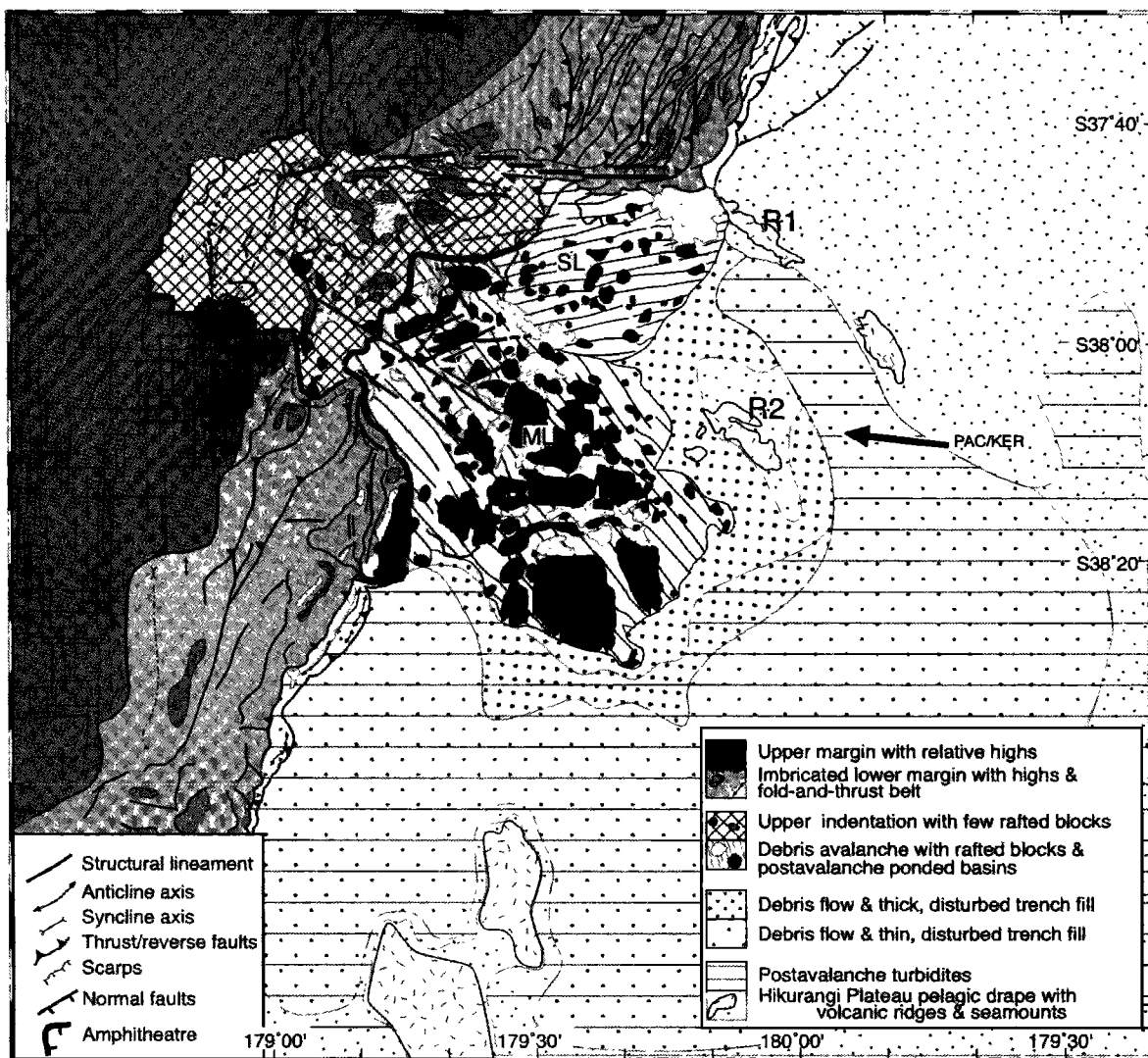


Figure 5. Generalized geological map showing main structural and gravity-controlled features including (1) saw-toothed segments of northern wall, (2) scalloped southern wall, (3) almost block-free upper indentation with folds and faults, some related to imbricated margin on either side, (4) scarp or amphitheater separating upper and lower parts of indentation, (5) lower indentation with rafted blocks and avalanche flow in two directions, ML, main lobe, SL, secondary lobe, (6) straight structural lineaments in lower indentation (see Figure 4 and Plate 1b) consistent with shortening along the PAC-KER convergence direction, and (7) seaward extent of avalanche, debris flow, and disturbed Hikurangi Trough fill, with covering of turbidites.

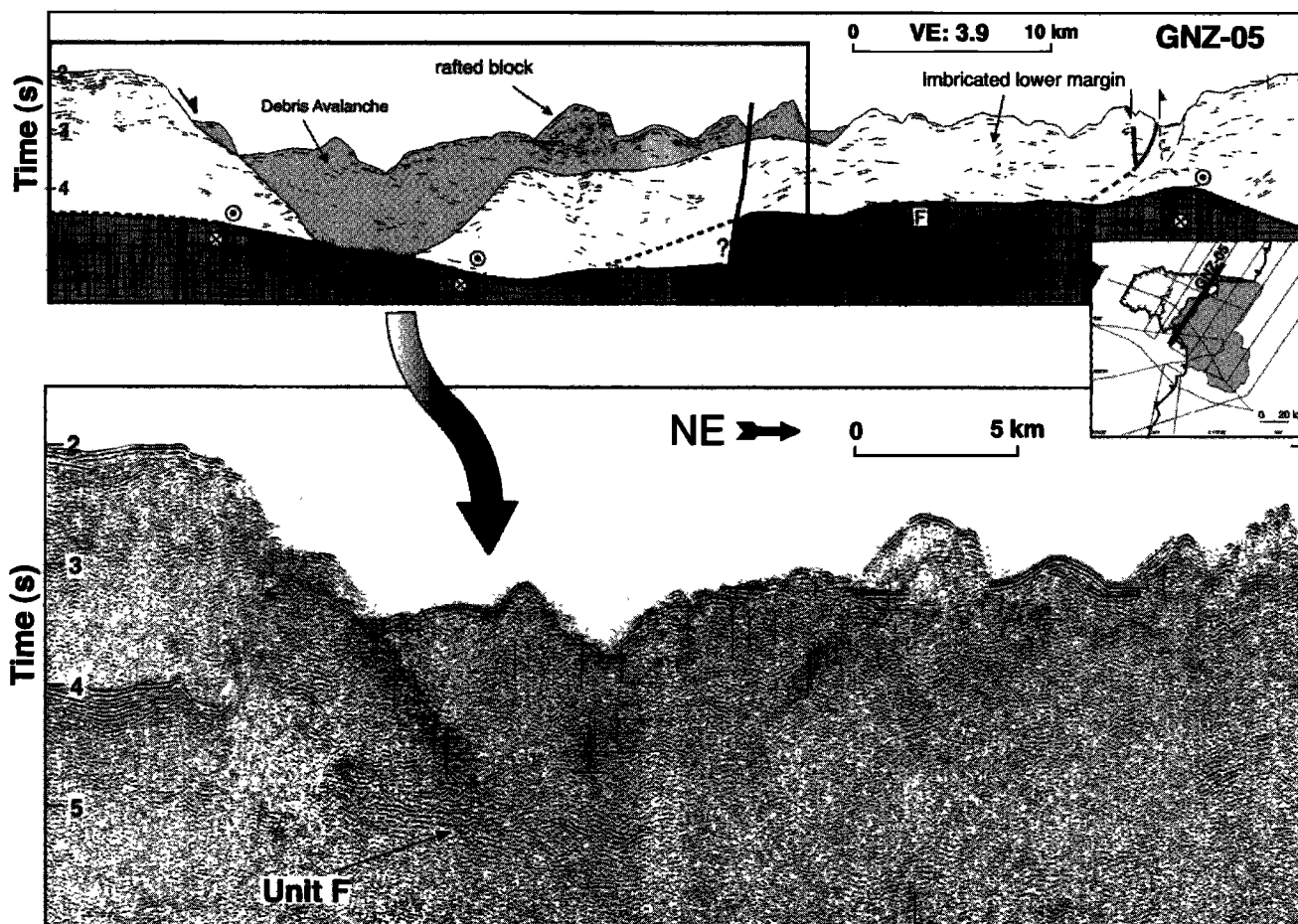


Figure 6. (top) GNZ-05 seismic reflection line drawing, with location (inset), showing (1) steep reverse faults through imbricated margin rock at the northern wall and (2) low-angle discontinuity between the southern wall and the debris avalanche. (bottom) Detail of a migrated section of the line showing debris avalanche with rafted block and unit F at the top of the subducting plate.

The lowest arcuate scarp reaches a height of over 1500 m with a northeastward dip of 25°. Seismic profile GNZ-05 (Figure 6) shows that this scarp continues to a depth of ~1.5 km beneath the seafloor in the form of a structural boundary marked by sharp reflection terminations that strongly diffract seismic energy. This structural boundary terminates at depth against a strongly reflective, well-bedded, and generally flat lying layer (unit F, Figure 6), which underlies both the indentation and the lower margin to the south. It is inferred that this layer is at the top of the subducting plate and represents preavalanche pelagic and possibly trench sediments thrust westward beneath the margin. Seismic line NZ-47 (Figure 8), which extends eastward across the scarp, shows the northern Hikurangi margin front to consist of imbricate thrust sheets that are sharply cut by the arcuate scarp. Shallow water, calcareous mudstones of lower Miocene to lower Pliocene age were dredged from the main imbricate thrust sheet outcropping at the scarp (Table 1). We interpret this scarp as a major scar left by blocks that collapsed in the avalanche.

4.4. Western Wall: Indentation Head

The western wall has subdued relief of only 200–300 m. It slopes at 4–10° and is incised by gullies and small rotational slumps. It trends N27°E, roughly parallel with the regional

bathymetric and structural trends (Figures 3 and 5). Its position along the continuation of major continental shelf faults suggests that its formation may have been structurally controlled. However, available seismic profile (Figure 9a) across this wall does not allow univocal determination of faulting type.

4.5. Avalanche-Free Upper Indentation

The relatively smooth upper part of the indentation is generally less than 1700 m deep, although along the northern margin, it extends down to 3300 m deep (Figures 3 and 5). Its topography is depressed by 400–800 m below the margin on either side (Figure 3). The upper indentation has only a few hummocks interpreted as slide blocks suggesting a largely avalanche-free topography. Most of these blocks appear to have detached from scarps inside the upper indentation, but some could have come from the scalloped southern wall (Figures 3 and 5). The upper indentation's northern half is characterized by ridges and basins trending subparallel to the northern wall. Seismic line 2044 (Figure 7) shows that the ridges are thinly stratified, southeastward tilted blocks bounded by normal faults, which, together with the block's depressed topography relative to the adjacent shelf, indicate a general subsidence controlled by southeastward extension.

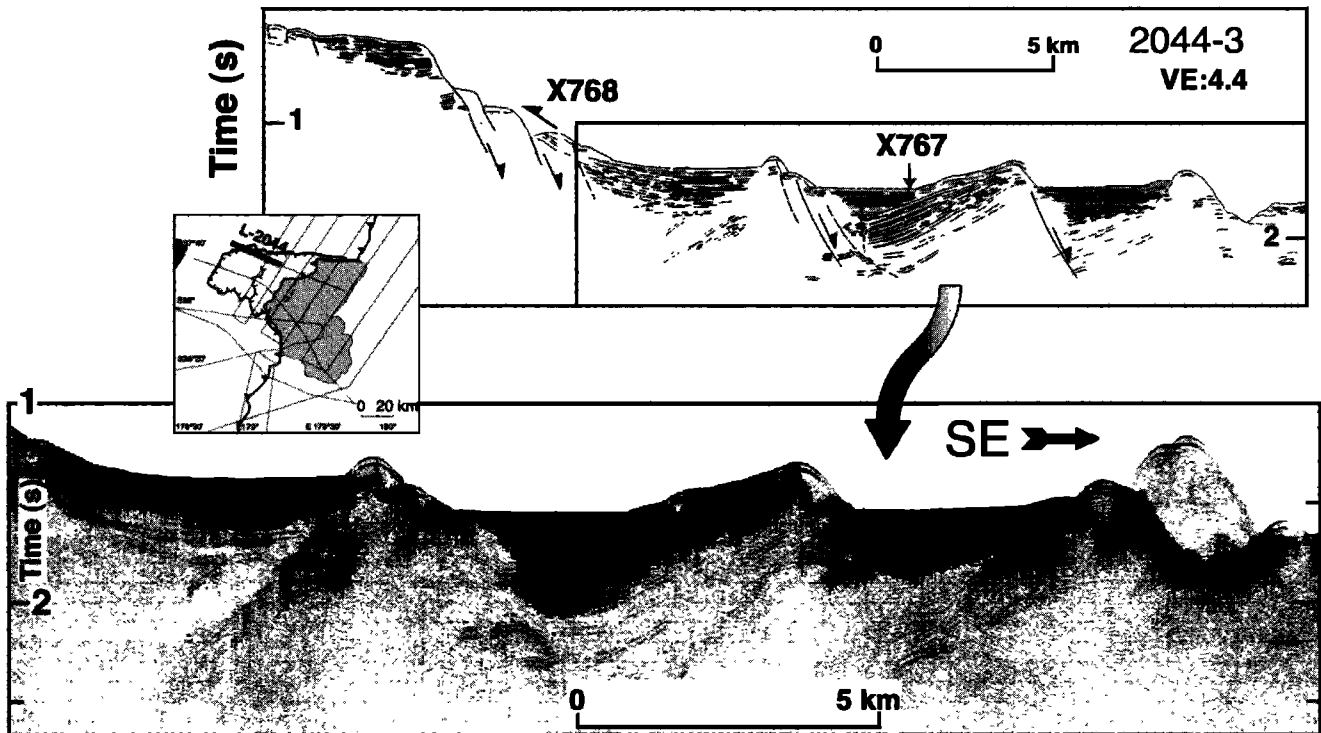


Figure 7. (top) The 2044-3 seismic reflection line drawing, with location (inset) showing rotated blocks, separated by normal faults, with subsequent basin fill. Central and left basins show sharp distinction between rotational block and basin fill. X767 and X768 are core and sample locations; see Tables 1 and 2. Right basin shows continuing rotation during basin fill. (bottom) Detail of single-channel seismic data.

The northern flanks of the tilted blocks are unconformably overlain by horizontally bedded, thinly stratified sedimentary wedges, which are ~250 m thick and formed mainly after tilting had ceased. The lower wedge has, however, recorded continuing block rotation during fill deposition. We conclude that the northern half of the upper indentation has subsided and that subsidence has now largely ceased.

The upper indentation's southern half consists of two broad benches at 600–1100 m deep and 1500–1700 m deep, separated by a seaward concave scarp centred on 1300 m (Figures 3 and 5). Both benches are underlain by sedimentary basins over 1.2 km thick (Figures 9a and 9b). The basins contain strongly reflective and well-stratified sequences overlain and locally intermingled with a seismically incoherent layer of variable thickness (~50–300 m). This layer is unconformably blanketed by 50–100 m of recent reflective deposits. The basins are deforming now by downslope extension, but earlier compression is indicated by an anticline near the lower basin's eastern boundary (Figure 9b). The anticline's crest has been eroded and unconformably overlain by a veneer of flat-laying basin sediments indicating that it is no longer active. On the basis of multibeam bathymetry, the anticline's axis trends ENE, which would suggest a westward compressive stress field (Figure 5). Low-amplitude folds also occur in basin fill in the upper basin (Figure 9a). Active extension is documented by east dipping normal faults N and G (Figures 9a and 9b). Fault N, which bounds the upper edge of the upper basin, cuts a wide antiform, displacing strong reflectors. The fault deforms the seafloor, and its recent activity is recorded on the downthrown side by a rotational sedimentary basin. Fault G, which is located between the upper

and lower basins, displaces both the seafloor and a 300-m-thick, seismically transparent layer that outcrops on the hanging wall of the fault. Rock sample X280 (Table 1) from this scarp is mid-Miocene calcareous mudstone. Thus our data indicate that in the southern half of the upper indentation, early compression has been followed by extension that is still active.

4.6. Avalanche-Covered Lower Indentation

Most of the lower part of the indentation is depressed more than 1 km below the margin on either side and is blanketed by a blocky avalanche deposit described in section 5. The lower and upper parts of the indentation are separated by the prominent 400–600 m high, 7–8° eastward dipping midslope scarp which, together with the lowest scarp of the indentation's southern wall, forms a 30-km-wide amphitheater (Figure 5). The amphitheater is regarded as the main avalanche headwall scarp. Seismic reflection line NZ-47 (Figure 8) supports this interpretation, and seismic line GNZ-05 (Figure 6) suggests a total scar height of as much as 2.5 km. Farther north the failure surface is less pronounced and appears mainly as an unconformable stratigraphic contact between the margin and avalanche deposits. Seismic line 3044-37-3 (Figure 9c) crosses the midslope scarp and shows a seaward dipping boundary joining it to the top of the subducting sediments (unit F in Figure 9c inset). Landward dipping, margin reflectors below this boundary contrast with seaward dipping avalanche reflectors above it. Although not outlined by a major reflector, the boundary is considered to be part of the avalanche failure surface.

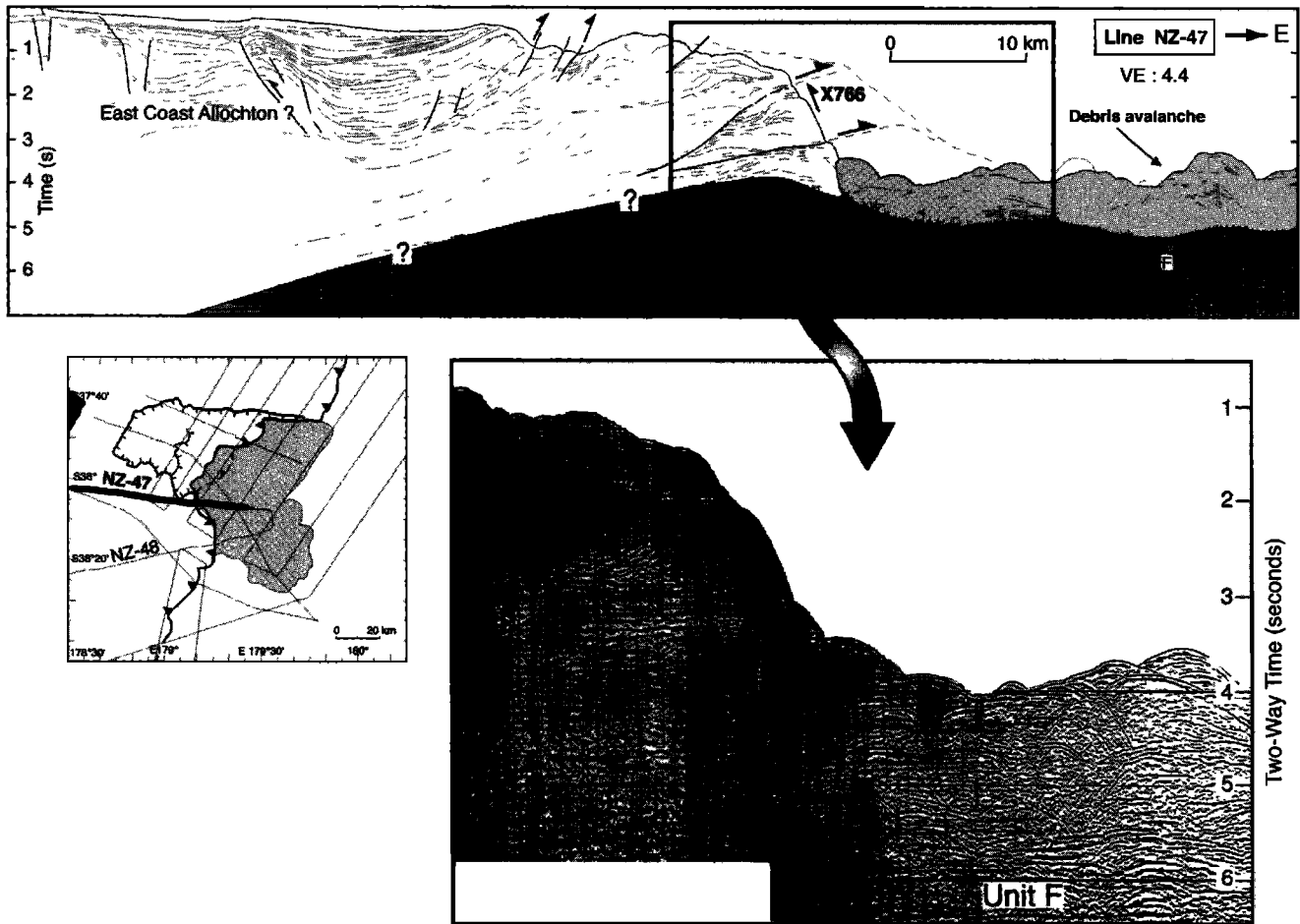


Figure 8. (top) Gulfrex NZ-47 seismic reflection line drawing with location (inset) showing imbricate margin lacking a recent accretionary wedge. The margin possibly includes the Paleogene allochthonous mass that outcrops onshore, obducted over well-bedded sediments containing a Miocene microfauna (sample X766, Table 1) and covered by a basin fill sequence with thrusting and backthrusting. The margin front is marked by a scar left by blocks that collapsed in the avalanche. Dashed lines are projected structures from line NZ-48 (see inset) suggesting collapsed blocks. Right side shows debris avalanche deposit. (bottom) Detail of a stacked section showing imbricated margin, avalanche scar, and debris avalanche.

Northeast of the amphitheater, the lower indentation is a 3600-m-deep reentrant of the Hikurangi Trough into the margin (Figure 4). The reentrant is bounded to the north by the N276°E trending northern wall (Figures 3 and 4), landward by a 12° eastward dipping slope, and to the south by avalanche deposits. Seismic lines GNZ-06 and GNZ-11 (Figures 10 and 11) indicate that the reentrant is underlain by ~100 m of turbidites above 300-500 m thick avalanche deposits.

5. Debris Avalanche Deposit

The avalanche deposit consists of a main lobe trending N155°E, and a northeastern secondary lobe trending N80°E (Figures 3 and 5). The secondary lobe has a hummocky surface with 30-40 small-sized hummocks (1-5 km across) and a topography that steps down toward the northern wall. The body of the secondary lobe has short, irregular reflectors that extend beneath the deep water reentrant (Figure 10). It is inferred that this northern lobe was prevented from entering the Kermadec Trench by a basement ridge (R1 in Figure 5) that acted as a dam to both avalanche and later turbidity currents.

The main lobe of the avalanche deposit has ~70 hummocks more than 1 km across, including at least 20 hummocks 5-18 km across. The lobe extends 70 km seaward from the midslope scarp to ~40 km seaward of a line joining the deformation fronts on either side. In several places, small enclosed basins between large blocks have flat-lying and parallel-bedded sediments that are generally 80-120 m thick. In plan view, large hummocks represent ~30% of the total area of the avalanche. On the basis of their distribution and size, proximal and distal areas of the avalanche can be recognized.

The proximal area is mainly landward of a line joining the deformation front on either side. It represents ~60% of the total avalanche area and is characterized by hummocks that are smaller than in the distal area and by tectonic lineaments. The hummocks, ranging from 1 to 3 km across and from 50 to 350 m high are predominantly located in the secondary lobe (Figures 3, 5 and 10). Others hummocks, located in the main lobe, are elongated and form ridges, 5-9 km in length, trending consistently ~N60°E along short structural lineaments. Some hummocks align subtransversally to the margin, along two remarkable structural lineaments, trending

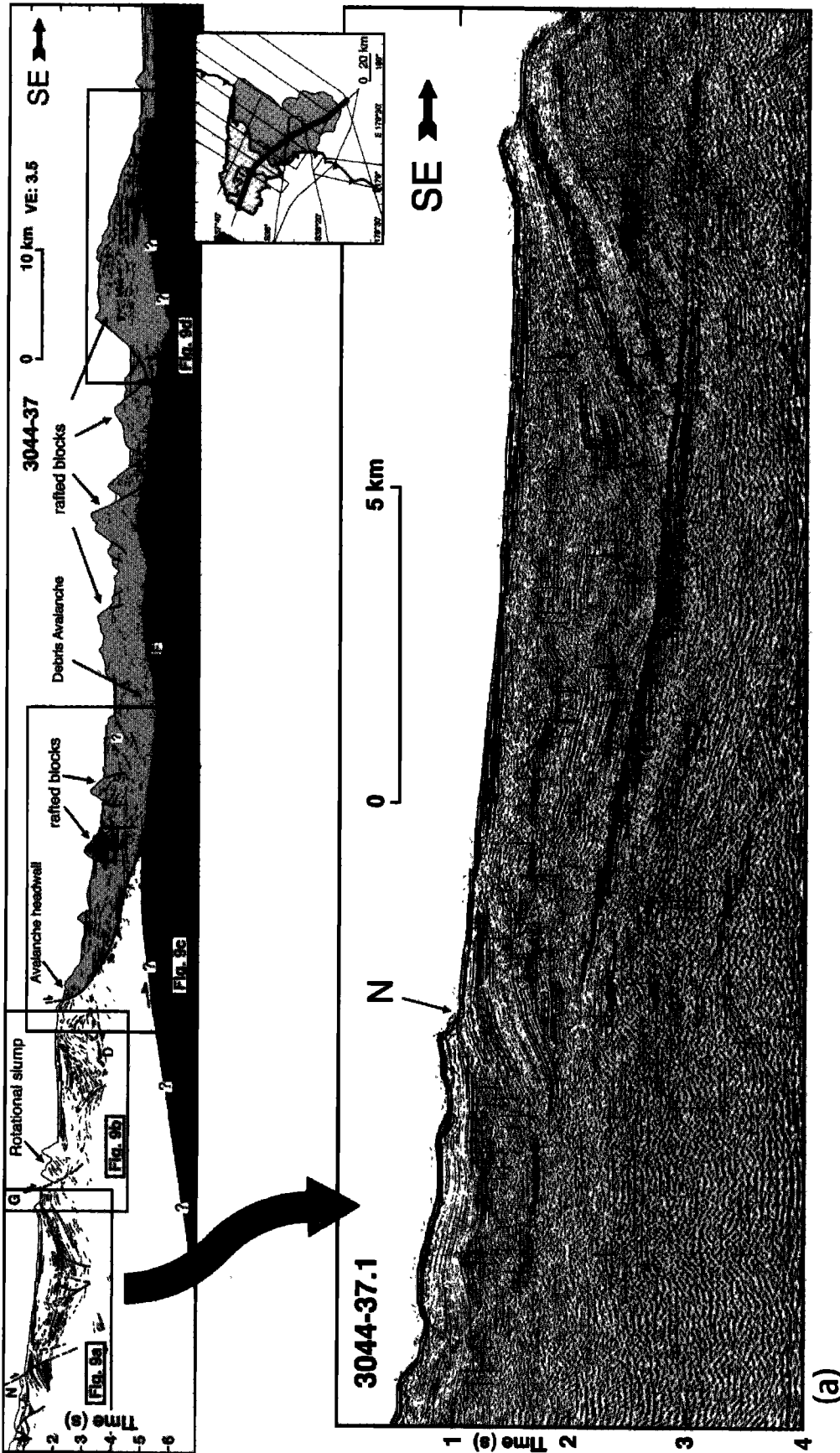
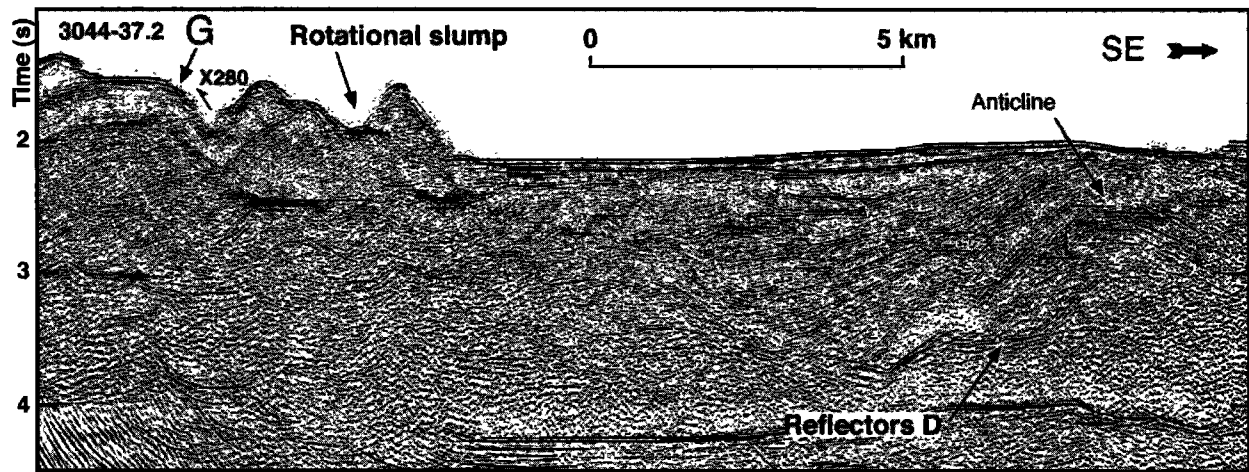
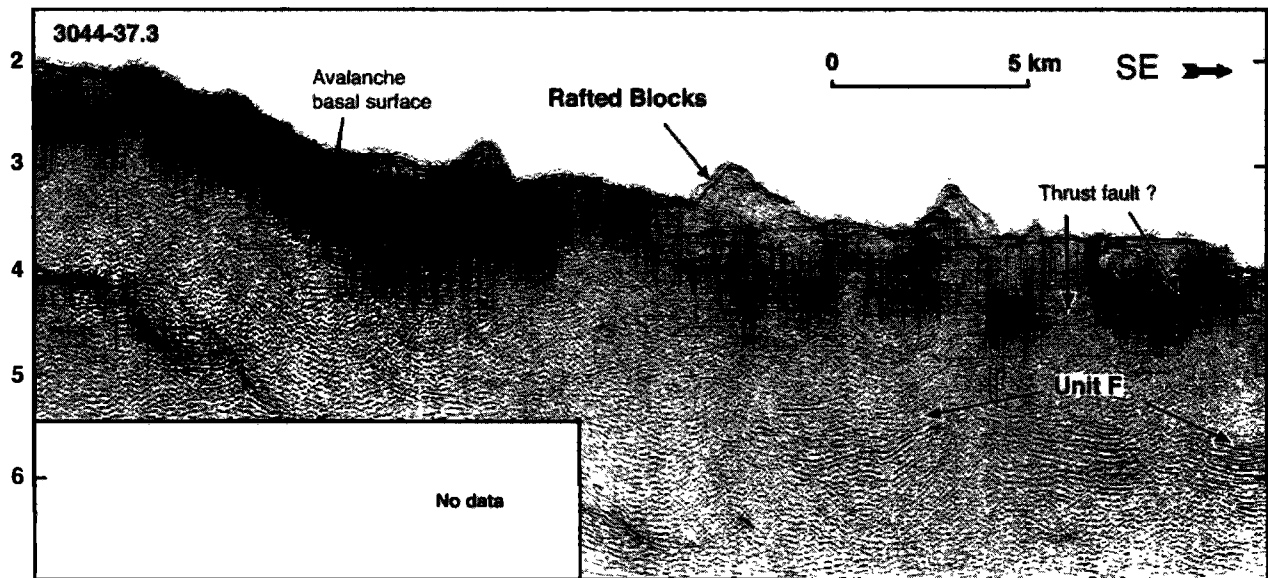


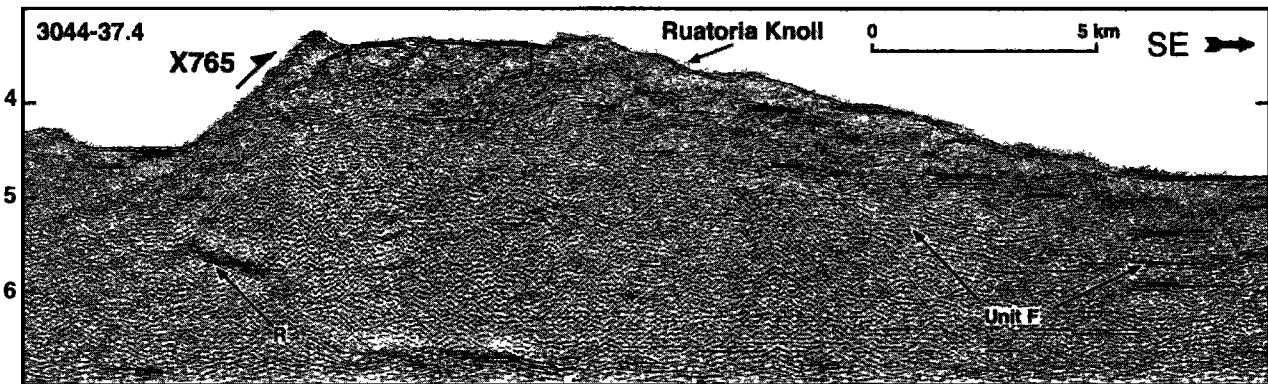
Figure 9. (a) (top) The 3044-37 seismic reflection line drawing down Ruatoria indentation and across Hikurangi Trough, with location (inset), contrasting downfaulted upper indentation with debris avalanche deposit on lower indentation and across trough. (bottom) Detail of migrated multichannel seismic data across upper indentation with upper of two sedimentary basins deformed by active normal fault N; basin sediment include a transparent layer interpreted as a debris flow. (b) Detail of seismic data across lower of two upper indentation basins with seaward anticline unconformably overlain by recent sediment, normal fault G, X280 sample location (Table 1), and basin transparent layer interpreted as a thin debris flow. Strong reflector D, which cuts the base of the anticline, could be the top of a subducting seamount. (c) Detail of seismic data across upper part of avalanche deposit downslope from main headwall showing small, well-bedded rafted blocks and incoherent reflections from the avalanche mass overlying strongly bedded unit F interpreted as preavalanche trough fill. Postavalanche shortening may be indicated by landward dipping thrust faults. (d) Detail of seismic data across largest avalanche block, Ruatoria Knoll, above strongly bedded unit F at leading edge of avalanche deposit, showing the imbricate sedimentary nature of the block. X765 sample data are given in Table 1. Reflector R is possible base of block.



(b)



(c)



(d)

Figure 9. (continued)

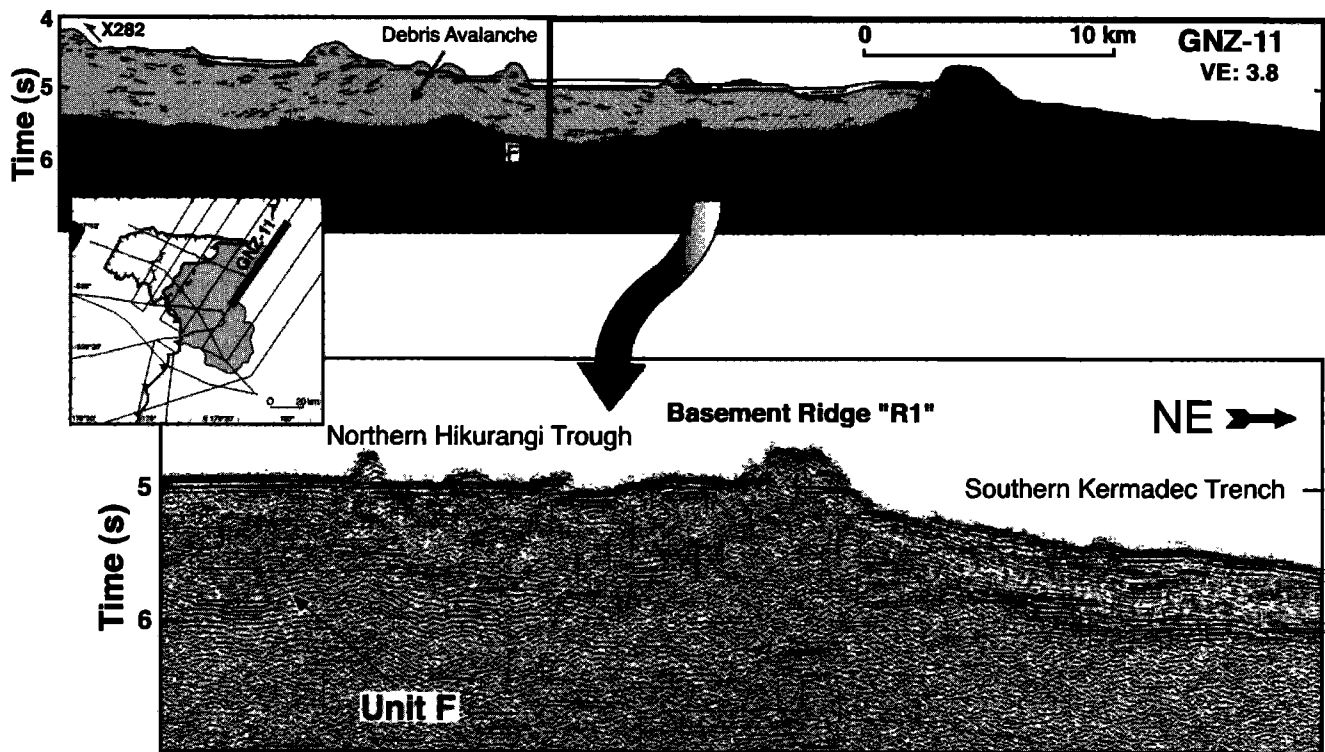


Figure 10. (top) GNZ-11 seismic reflection line drawing, with location (inset), showing avalanche deposit of the secondary lobe being blocked by a basement ridge that prevents passage to the Kermadec Trench. X282 sample data are given in Table 1. Thin turbidite fill overlies the avalanche deposit south of the ridge. (bottom) Detail of a migrated section of the line.

N125°E on the average and offsetting the seafloor of the proximal area. The longest of the two lineaments extends 10 km inside the upper indentation. A N150°E trending, 25-km-long lineament, also deforms the proximal avalanche deposit and cuts the upper indentation. These lineaments postdate both the indentation and avalanche deposit. Seismic reflection profiles GNZ-05 (Figure 6), L-37-3 (Figure 9c), and GNZ-06 (Figure 11) across the proximal avalanche show generally incoherent reflections overlying unit F, a strongly reflective layer with distorted, near-parallel bedding. This layer, which extends beneath the entire avalanche mass and to seaward in the Hikurangi Trough, is generally ~0.6 s two-way time (tw) thick and can be recognized at a similar depth beneath the margin south of the Ruatoria indentation. We interpret unit F as pelagic drape perhaps with a cover of preavalanche trough fill [Lewis *et al.*, 1998]. The top of unit F is inferred to mark the base of the avalanche. On basis of this interpretation, the maximum avalanche thickness, assuming a sound velocity of 2000 m s⁻¹ is ~1.7-2.0 km (Figure 9c). Despite the general absence of coherent bedding in the avalanche deposit, some hummocks return well-bedded, high-frequency reflections, with clear lateral boundaries, that clearly delineate thinly stratified and gently deformed blocks (Figure 11). These blocks are isolated in the avalanche matrix, and they appear to be rooted at a depth of 0.8-1.2 km beneath seafloor. The internal structure of some blocks (Figure 11) resembles that of the anticline in the upper part of the indentation (Figure 9b). We infer that the vast majority of blocks located in the proximal area are rafted, having slid from the midslope scarp or the southern wall.

The distal part of the avalanche, which is seaward of the deformation front on either side, represents 40% of the avalanche surface. It includes a cluster of mega blocks. Five of them exceed 10 km in their greatest dimension and reach altitudes > 600 m above the surrounding seafloor. The largest block, which is 18 km long, 1200 m high above the adjacent seabed, is the most distal and has been named Ruatoria Knoll. It has undulating reflectors, with gentle, landward apparent dips (Figure 9d) and [Lewis and Pettinga, 1993], indicating a deformed sedimentary structure, similar to that of imbricated sediments on the adjacent margin (Figure 8). Strong reflector R at a depth of 5.5 stwt beneath the Ruatoria Knoll's northwestern flank may be either the base of the block or a side echo. However, if unit F, which extends beneath its southeastern flank is extrapolated beneath the knoll toward reflector R, then the block's maximum thickness is ~2.5 stwt. Dredged samples from the northeastern face of the Ruatoria Knoll consist of mid-Oligocene to mid-Miocene calcareous mudstone from mainly upper slope environments (Table 1). Essentially similar rocks and fauna were dredged from the walls of the indentation, including the steep scarp at the eastern end of the southern wall (Figure 8 and Table 1). Lithologies and faunas in the blocks are completely different from those that occur in the pelagic drape of oceanic seamounts [Lewis and Bennett, 1985], and the samples are proof that even the largest blocks were derived from the adjacent margin.

The shape and relative position of the blocks give an indication of the avalanche's direction of flow and pattern of emplacement. Blocks have remarkable morphologies of two

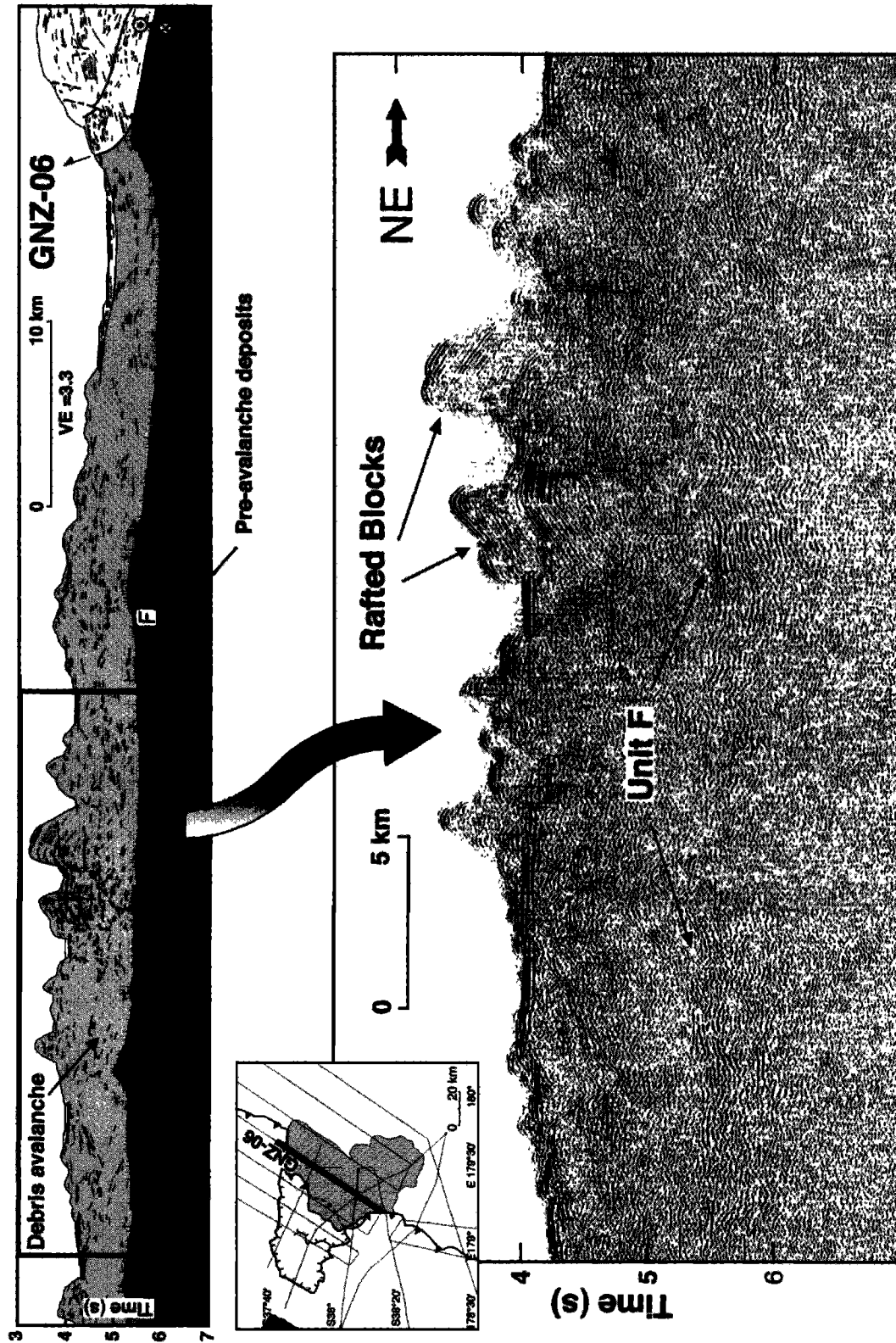


Figure 11. (top) GNZ-06 seismic reflection line drawing across thick avalanche deposits, with location (inset), showing large, thinly stratified, rafted blocks over the strongly bedded, preavalanche deposit, unit F. (bottom) Detail of a migrated section of the line.

main types. The more distal ones are angular and asymmetric in map view and cross section. For example, the Ruatoria Knoll, is rhomboidal in plan view with a gently dipping and convex southern flank and three linear and steep sides. We infer that the gentle convex flank, now inclined toward N215°E, represents the original surface of the lower Hikurangi margin. If indeed this is the original margin slope, then the block has rotated 90° clockwise, from its original dip toward N215°E. Significantly, the three steep sides mirror similar, steep, linear flanks of neighboring blocks, implying that all were once joined, perhaps as part of one even larger block. Most obvious are the N150°E trending, parallel walls between the Ruatoria Knoll and another large block to the east, suggesting that these parted at a very late stage. The N150°E alignment of the block's walls and the longest axis of the main lobe reflect the trajectory of the avalanche. Other nearby large blocks have different morphologies. They show multiple summits and narrow crests, flanked by locally steep but smooth slopes that are concave in cross section. This morphology may reflect disintegration of heavily fractured rocks. Some of these blocks are aligned subparallel and some near perpendicular to the inferred N150°E direction of transport. The matching and alignment of peaks and blocks could indicate that one massive block, possibly as large as 20 by 35 km, detached from the margin, breaking up, rotating, and leaving detached smaller blocks at the avalanche's trailing edge, as it traveled down the slope and for 40 km across the Hikurangi Trough.

6. Debris Flow Deposit

A seismically transparent layer, which extends beneath the Hikurangi Trough for up to 100 km in front of the debris avalanche deposit (Figure 5) and covers ~8000 km², is inferred to be a debris flow deposit associated with the blocky avalanche. Seismic lines GNZ-14 (Figure 12) and 3044-38 (Figure 13), which cross the Hikurangi Trough ahead of the avalanche, show five seismic units overlying the Hikurangi Plateau acoustic basement. The deepest unit is the strongly reflective unit F recognized beneath the avalanche mass. A 0.3 stwt thick weakly reflective, parallel-bedded unit (unit T) is overlain by a set of strongly reflective layers (unit X), which in turn are irregularly overlain by the 0.1-0.2 stwt thick transparent layer (unit DF). Unit X contains numerous limited but well-stratified reflectors that have different dips and locally clear evidences of disturbance. The base of unit X is commonly, but not universally, recognized at a strong reflector at the top of unit T. Unit DF shows no coherent reflections, and both its upper and lower surfaces are irregular. Its upper surface is unconformably overlain by the most recent, 0.2 stwt thick and well-stratified unit PAT interpreted as postavalanche trough turbidites. We interpret the transparent unit DF as debris flow deposit and unit X as preexisting trough fill disturbed by passage of the debris flow or by dewatering after rapid loading by the debris flow deposit. Within ~20–30 km of the front of the avalanche deposit unit X increases in thickness from 350 ms to 800 ms twt, in places at a preexisting fault (Figures 5 and 12). We interpret this increase to result from extensive disturbance of trough sediments by the pressure or bow wave in front of the advancing avalanche. Seismic line 3044-38 (Figure 13) shows that the debris flow and the other units younger than unit T

were recently shortened. Shortening appears to have initiated by backthrusting these units against the toe of the margin, and then a thrust fault propagated seaward, creating an incipient accretionary lobe.

7. Discussion

7.1. Indentation and Slope Failure: Results From a Two-Stage Process

The structural data presented above indicate that the Ruatoria indentation and slope failure are genetically linked. However, they are not synchronous and did not result from the same process. The similarities between geological structures within the Ruatoria upper indentation (Figure 9) and those of the Hikurangi upper margin immediately to the south (Figure 8) support the idea that the depressed upper indentation seafloor reflects local subsidence of the margin and is generally not the avalanche failure surface. Sedimentary basins within the upper indentation are the northern continuation of the imbricated Neogene and Quaternary shelf basins to the south (Figures 5 and 8). The 500-800 m amount of subsidence together with preservation of coherent geological structures in the subsiding basins, inversion from compressional to extensional tectonics, and ceased extensional faulting in the northern half of the upper indentation (Figure 7) and continuing extension (Figure 9a) in its southern half attest to a relatively slow subsidence process. In contrast, the cleanness of the avalanche scar along the indentation's southern wall, the avalanche dislocation pattern, and the blocky angular morphology, as well as the fact that the largest block slid farthest away from the margin on an horizontal seafloor, attest to high energy transport and therefore a catastrophic collapse. We conclude that most of the Ruatoria indentation formed first by subsidence, whereas avalanche and debris flow occurred later on, instantaneously.

7.2. Causes of Instability on the Northern Hikurangi Margin

Both the subsidence in the Ruatoria indentation and the catastrophic collapse reflect large-scale submarine instability within consolidated rocks of the Hikurangi margin. Several regional factors may contribute to this.

The heterogeneous East Coast Allochthon is a regional factor of instability. Onshore, allochthonous sheets of fractured Cretaceous to Paleogene sediments and seamount blocks up to 2 km thick [Field *et al.*, 1997; Rait, 1995; Stoneley, 1968] are buried by Neogene sediments up to 4 km thick [Field *et al.*, 1997]. To date, there is no clear evidence of the extent of the allochthon and covering beds offshore. However, we interpret margin strata with discontinuous reflectors and evidence of thrusting (Figure 8) as a possible eastern continuation of the allochthon. Overlying, well-bedded, gently folded and reverse faulted basin sediments are Miocene to Recent cover beds. Parts of the allochthon to the northwest were subject to Miocene gravitational remobilization [Hayward, 1993], and these parts are so fragmented that they have been variously referred to as olistostrome, wild flysch, megabreccia, and chaos-breccia [Bradley, 1964; Kear and Waterhouse, 1967]. We suggest that its remobilization can still form "chaotic" deposits.

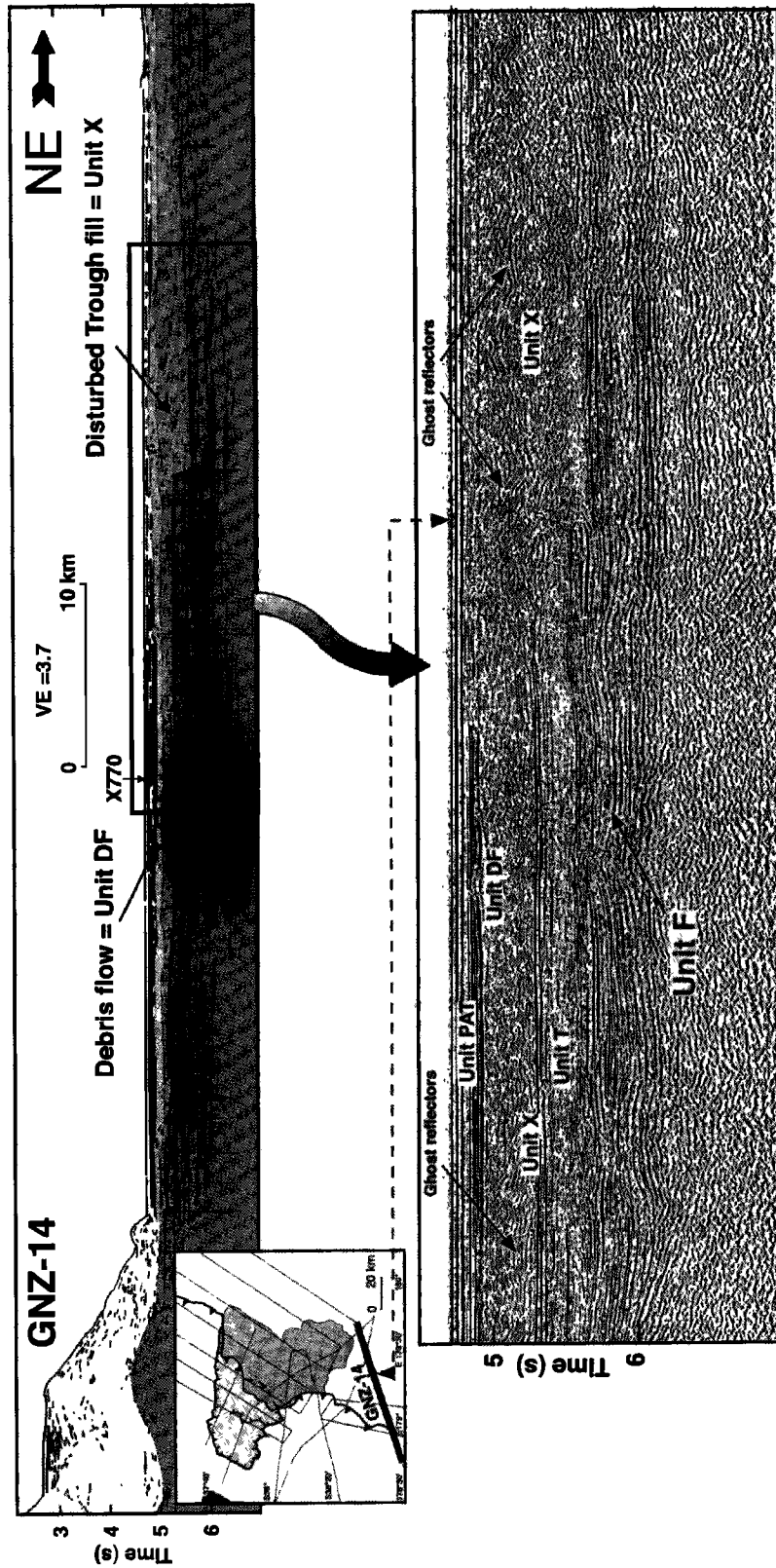


Figure 12. (top) GNZ-14 seismic reflection line drawing, with location (inset), across northern Hikurangi Trough, showing transparent debris flow, with underlying “ghost” reflectors from deformed turbidite beds. Deformed trough sediments are much thicker northeast of a fault close to the avalanche deposit; X770 core data are given in Table 2. (bottom) Detail of a migrated section of the line close to the avalanche deposit showing, from base, strong reflectors of unit F, weakly reflective unit T, strongly bedded unit X, which is mainly deformed, and the debris flow DF with its irregular upper surface overlain by the strongly bedded postavalanche turbidites (PAT).

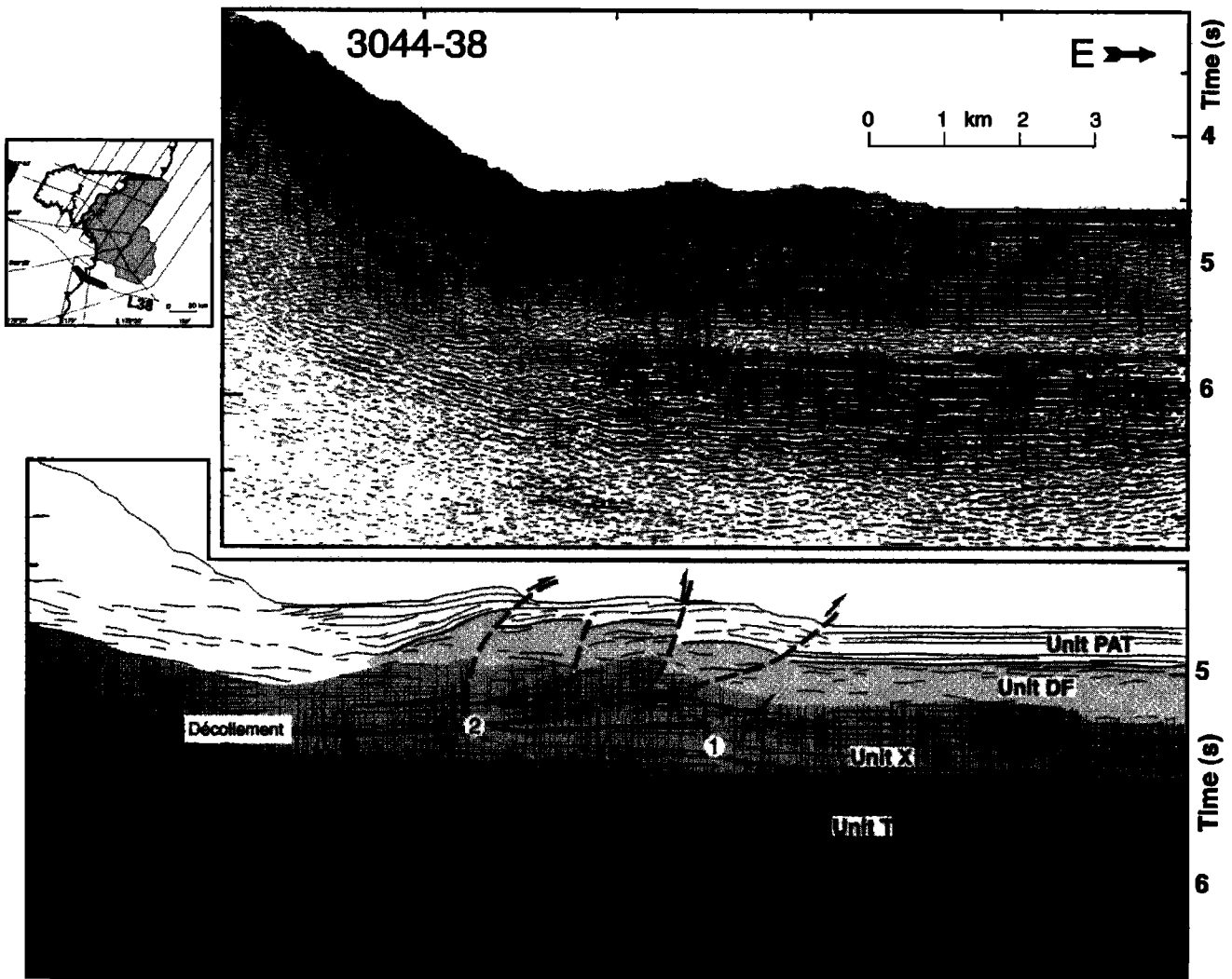


Figure 13. (bottom) The 3044-38 seismic reflection line drawing, with location (inset), across northern Hikurangi Trough, showing shortening of the trough sediment including debris flow, against the toe of the margin. A backthrust (1) cut by a seaward verging thrust (2) suggests a two-stage shortening with a total shortening of near 3.2 km; units are as defined in Figure 12. (top) Detail of a migrated section of the line.

Throughout the east coast region, an Eocene bentonite layer is renowned for its high fluid pressures and low shear strength [Mazengarb, 1998]. It forms the main detachment horizon for the allochthon and lubricates shearing within it [Field *et al.*, 1997]. This highly mobile mud may be squeezed into overlying sequences and erupts at the surface as mud volcanoes [Ridd, 1970; Stoneley, 1962]. It is inferred to lubricate normal faults downthrown toward the trench [Mazengarb, 1998]. If, as suspected, the bentonite layer underlies the margin offshore, then it will continue to represent a significant source of instability.

The risk of gravitational failure in already fragmented deposits and at low strength horizons may have significantly increased because of regional seaward tilting. This tilting results from rapid rise of mountain ranges onshore [Walcott, 1987] and subsidence caused by tectonic erosion by the downgoing plate on the lower slope [Collot *et al.*, 1996]. Micropaleontological evidence indicates that most rock samples were dredged from water depths much deeper than their

original environment of deposition (Table 1), supporting downwarping of the slope since Miocene times.

High fluid pressure, particularly from gas, dramatically reduces the shear strength of susceptible layers [Hampton *et al.*, 1996; Papatheodorou *et al.*, 1996], and much of the Hikurangi margin is percolated by methane-rich fluids derived from subducting sediments [Katz, 1981; Lewis and Marshall, 1996]. In general, the porosity of thin subducting sediments is higher than the average porosity of thick subducting sediments, particularly if the top of the thick sequence is frontally accreted [Lallemand *et al.*, 1994]. Thus high fluid flow might be expected on the northern margin, where thin, water-rich turbidites are wholly subducted, compared with the southern margin, where thick turbidites are off-scraped and frontally accreted [Davey *et al.*, 1986; Lewis and Pettinga, 1993]. In addition, bottom-simulating reflectors attributed to gas hydrate occur widely on the Hikurangi margin [Field *et al.*, 1997; Katz, 1982]. Gas hydrates can become unstable and dissociate into water and 170 times their own volume of free

gas, particularly during the release of hydrostatic pressure associated with falling sea-level [Lerche and Bagirov, 1998]. This drastically reduces the shear strength of many slope sediments [Hampton et al., 1996] and is a potentially destabilizing influence on at least shallower parts of the avalanche

7.3. Origin of the Indentation and Avalanche: Results of Oblique Seamount Subduction

The Ruatoria avalanche and indentation are not a result of simple slope failure. There is compelling evidence that they are a response to oblique subduction of a seamount.

7.3.1. Criteria used to recognize seamount impact. Subducting seamounts have produced indentations in convergent margins around the world. Their passage beneath margins causes compression with back thrusts ahead of the asperity, uplift above it, and "tunneling" and collapse in their wake [Dominguez et al., 1998; Lallemand and Le Pichon, 1987; Lallemand et al., 1994; Masson et al., 1990; von Huene and Lallemand, 1990]. Impacting seamounts produce first a U-shaped reentrant in the accretionary wedge deformation front, then a semicircular depression in the lower margin, and finally an elongated groove-like indentation of the whole margin. In a non accretionary margin the groove is generally flanked by subparallel scarps that trend parallel to the plate convergence direction. Such spectacular impacts were imaged across the Costa Rica margin [von Huene et al., 1995]. The indentation may remain long after the seamount that caused it has passed, and it may accumulate flat-laying sediment and minor slope failure deposits [Collet and Fisher, 1989]. Experimental modeling shows that when the seamount underthrusts the cohesive part of the margin, subsidence initiates above the seamount trailing flank: former back thrusts are then reactivated into steep normal faults controlling the indentation subsidence [Dominguez et al., 2000]. Seamount subduction is also shown to bulldoze material from the front to beneath the inner part of the margin, thus accounting for the rocks missing in the indentation [Dominguez et al., 2000].

7.3.2. Impact criteria applied to the Ruatoria indentation. Such geometrical and morphostructural characteristics can be recognized in the Ruatoria indentation clearly revealing the structural imprint left by a subducted seamount. First, the northern wall of the indentation, which cuts linearly across the entire margin and parallels the PAC-KER plate convergence direction, is inferred to be one side of a long, groove-like indentation formed by a subducting seamount. Second, the upper part of the indentation reveals the existence of compressional and extensional structures associated with the seamount passage. Third, the 3600-m-deep margin reentrant (Figure 4) at the seaward end of the northern wall denotes removal of margin material that we believe has been pushed and dragged beneath the margin by the seamount. Fourth, the compacted volume of the indentation is larger than the compacted volume of the avalanche as discussed in section 7.7 (Table 3).

7.3.3. Size and shape of subducted seamount. The shape of the indentation and the margin's deformation pattern depend upon both the margin and seamount geometry and rock properties [Dominguez et al., 1998]. Experimental modeling indicates that the seamount impact groove's lateral scarps are better expressed in a cohesive margin than in an accretionary wedge and that the groove's width approximately

equals the seamount diameter, especially if it is large and flat-topped. Oceanic seamounts closest to the Ruatoria indentation are large, flattish-topped and elongated N155°E. We suggest that a seamount of similar size (~35-40 km long), shape, and orientation to Gisborne seamount (Figure 2) partly formed the Ruatoria indentation while subducting beneath the relatively cohesive but imbricated Hikurangi margin.

7.3.4. Present-day location and depth of the subducted seamount. Oceanic seamounts buried at shallow depth beneath an accretionary wedge have been either imaged from seismic reflection [von Huene et al., 1997] or, more often, indirectly identified by a magnetic anomaly [Barckhausen et al., 1998; Lallemand and Chamot-Rooke, 1986] or by a circular uplifted zone associated with the thrust of their summit [Dominguez et al., 1998]. The uplifted zone is incised by a divergent network of fine subvertical fractures and bounded landward by back thrusts [Dominguez et al., 1998]. These identification criteria are not met in the Ruatoria indentation, possibly implying that the seamount responsible for the indentation has already subducted too deep beneath the margin. Experimental modeling shows that normal faulting deforms the cohesive part of the margin above the trailing flank of the seamount, but activity ceases when the seamount has subducted far enough, past the indentation headwall scarp. Therefore active normal faulting within the upper part of the Ruatoria indentation (Figure 9a) indicates that the buried seamount lies somewhere beneath the shelf immediately landward of the indentation western wall. A comprehensive seismological study of interplate earthquake distribution beneath the adjacent land [Reyners et al., 1999] suggests that a seamount, if located beneath the shelf, would be 10-15 km deep, probably too deep to deform the overlying seafloor (Figure 14).

7.4. Timing of Avalanching and Northern Wall Formation

The avalanche and associated debris flow are shown to be younger than most of the indentation. Their age can be estimated from the thickness and sedimentation rates of cover beds in enclosed basins surrounded by avalanche blocks, and trough sediment overlying the debris flow. A 2.93 m core from one of the largest basins (X764 in Figure 2 and Table 2) contains mainly hemipelagic mud with 10 graded silt layers inferred to be turbidites derived from adjacent slopes. It also contains two air fall ash layers at 54-57 cm and 109-113 cm below the seabed that are correlated with 1.8 and 3.3 ka eruptions respectively, on the basis of the geochemistry of the glass. This indicates a Holocene rate of sedimentation of ~0.33 m kyr⁻¹. An accelerator mass spectrometer (AMS) radiocarbon age of 8775±60 years B.P. for planktonic foraminifers from the base of the core also gives a rate of 0.33 m kyr⁻¹, confirming this as a uniform rate for Holocene. Extrapolating the same rate to the base of the 120-m-thick basin would imply that deposition began there ~360 ka. South of the avalanche deposit, a 0.97-m core was recovered from 140-m-thick parallel-bedded trough fill overlying the debris flow (X770 in Figure 2 and Table 2). The core consists of four relatively thick silty turbidites with thin hemipelagic layers and ash layers at 61-64 cm and 94-97 cm below the seabed, identified as the same two 1.8 and 3.3 ka ash layers. With comparatively few but thicker turbidite layers compared with the enclosed basin on the avalanche, long-term deposition

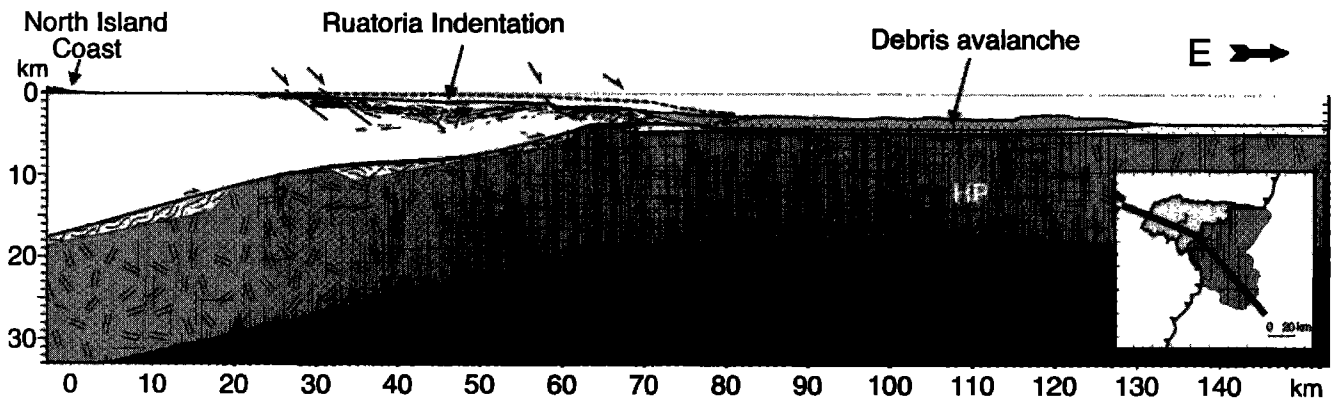


Figure 14. Interpreted crustal cross section through the Ruatoria indentation and avalanche, showing possible position of subducting seamounts. Location shown in inset. Interplate surface beneath North Island east coast after [Reyners *et al.*, 1999]; HP, Hikurangi Plateau thickness after [Davy, 1992]; dashed line is the inferred preindentation topography.

rates are difficult to estimate from short cores but are broadly similar to those in the enclosed basins.

Age extrapolations based on Holocene rates over-estimate the avalanche debris flow age as rates of terrigenous input to the continental slope were several times greater during glacial ages. A piston core from an enclosed basin on the lower Hikurangi margin 250 km south of the Ruatoria avalanche suggests that glacial age sedimentation rates were ~ 4 times faster than Holocene rates, due mainly to windblown dust and to an increased fluvial supply directly to the slope from a largely deforested landscape [Stewart and Neall, 1984]. However, a piston core from the same area indicates only a modest increase, perhaps only 50%, from the last interglacial age and falling sea level to the height of the last glacial age, with only a slight decrease into the Holocene (L. Carter *et al.*, pers. oral communication, 1999). Farther offshore, a core from the central part of the Hikurangi Plateau showed a threefold increase in the last glacial age sedimentation accumulation rates with respect to that of the Holocene. If the threefold to fourfold increase for glacial ages were correct, then a rough median rate for the Late Quaternary based on sea level curves, might be $\sim 0.7 \pm 0.1$ m kyr⁻¹. Considering a 120 ± 12 m thick enclosed basin, we derived an age for the avalanche of $\sim 180 \pm 40$ ka.

A 3.81 m core recovered from one of the small basins near the western end of the indentation's northern wall (X767, Figure 2 and Table 3) helps to constrain its age there. An AMS age of 1999 ± 60 years B.P. for planktonic foraminifers from the base of the core gives an exceptionally high sedimentation rate of 1.9 m kyr⁻¹. However, for the last 1000 years or so, shelf deposition rates have increased significantly, following deforestation of the adjacent land after human occupation [Carter *et al.*, 2001]; the only available dates for deforestation on North Island's east coast appear to confirm the offshore record despite uncertainties regarding contamination [McGlone and Wilmhurst, 1999]. We estimate that an average sedimentation rate for glacial (deforested)–interglacial (usually forested) cycles might be $\sim 1.6 \pm 0.2$ m kyr⁻¹. Such a rate would imply that the 250 ± 25 m thick basin overlying a tilted block formed $\sim 160 \pm 30$ ka. Because of age uncertainties, we suggest that both the avalanche and block tilting occurred at $\sim 170 \pm 40$ ka.

7.5. Scenario for Oblique Margin Indentation and Slope Failure

Geometrical reconstruction and avalanche dating help to constrain the timing of the indentation and slope failure. According to the 54 km Myr⁻¹ PAC-KER plate convergence rate and N277°E direction and the presumed location of a large buried seamount beneath the continental shelf, it is inferred that the seamount impacted the margin between 2.0 and 1.3 Ma (Figure 15a). The 3600-m-deep margin reentrant formed as the seamount disappeared beneath the margin and probably acted as a sink for small slumps and debris flows that occurred in the wake of the seamount. Experimental modeling shows that when a seamount is being subducted, the interplate décollement is uplifted above the seamount roof and remains deflected upward above the seamount trailing flank, so that a shadow zone develops both in front of and in the wake of the seamount allowing frontal margin material and wake slump masses and trench fill to be pushed and dragged into the subduction along with the seamount (Figure 14) [Collot *et al.*, 1992; Dominguez *et al.*, 2000; Lallemand *et al.*, 1994]. We believe that this process accounts for the formation of the deep water reentrant of the Ruatoria indentation. Between 2 and 0.16 Ma, the subducting seamount cut a 30-km-wide groove-like indentation obliquely through the margin with uplift in front and subsidence behind the seamount. The groove and northern wall are diachronous. Because of oblique convergence, this process left an unstable triangular wedge in the acute angle between impact groove and the steep edge of a tectonically eroded margin (Figure 15b). This margin was already rendered unstable by seaward tilting of low strength Eocene clays and Miocene slide deposits and by percolating fluids. It required only a large earthquake, or disruption by subduction of another seamount, to cause the triangle to collapse at ~ 170 ka (Figure 15c). Unusually large earthquakes at a site predisposed to failure are commonly cited as the triggering mechanism for large submarine slope failures [Hampton *et al.*, 1996]. At the northern Hikurangi margin the plate interface is presently weakly coupled and accumulating strain is generally dissipated in numerous small earthquakes [Reyners and McGinty, 1999; Smith *et al.*, 1989]. However, the subduction of a large seamount may locally cause locking

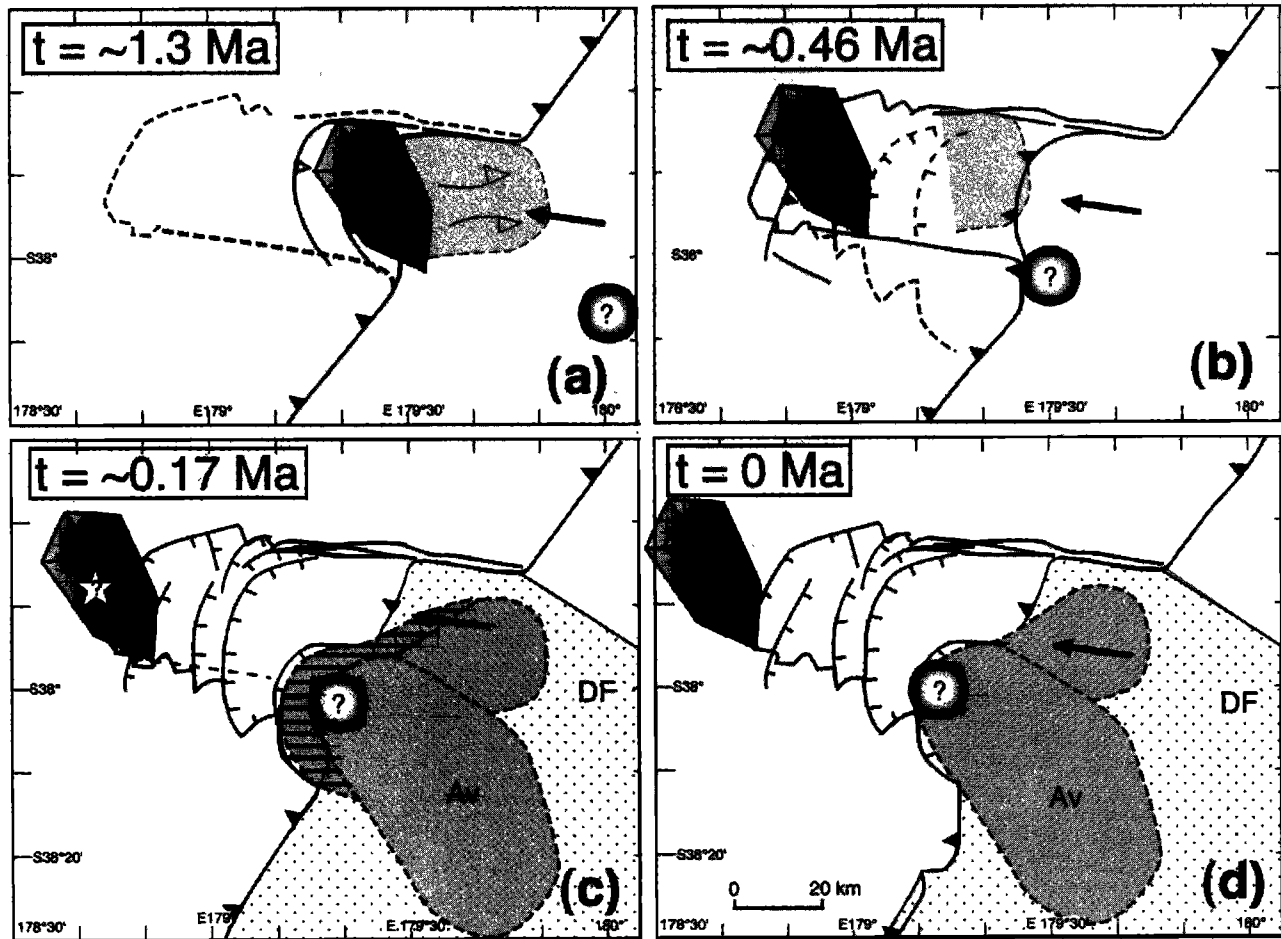


Figure 15. Scenario for formation of Ruatoria indentation and avalanche from 1.3 Ma to Present: (a) Initial impact of a large seamount similar to the Gisborne seamount and formation of the deep-water trough reentrant; (b) formation of the groove-like indentation, the unstable triangular wedge, and beginning of extensional faulting in upper indentation; (c) slope failure that resulted in avalanche (Av) and debris flow (DF) deposits triggered either by an earthquake (star ?) or/and a small seamount (?) detected as a magnetic anomaly; solid arrow is PAC-KER convergence vector; hatched area is avalanche deposits that is subsequently shortened or subducted; (d) present-day situation with large seamount buried 10-15 km beneath the shelf (Figure 14).

of the plate boundary sufficient to generate large earthquakes [Cloos, 1992; Scholz and Small, 1997]. The large seamount that incised the indentation may have generated earthquakes large enough to cause the wedge failure. In addition, deformation by a small seamount identified from magnetic anomalies [Collot and Davy, 1998, Figure 16] near the indentation's southern wall (Figure 15c) may also have helped the collapse. Reflector D from seismic line 3044-37 across the midslope scarp (Figure 9a and 9b), which appears to truncate the base of an anticline, could be the top of the small subducting seamount. This scenario implies that the indentation's southern wall and avalanche are younger than most of the indentation. However, dating of overlapping, horizontal strata on tilted blocks (Figure 7) near the western end of the northern wall indicates that a rotational collapse occurred in the upper indentation at about the same time as the avalanche, i.e., $\sim 170 \pm 40$ ka. Thus the overall data set can be interpreted to suggest that the slope failure that caused the avalanche, released stress in the margin, thus producing headwall collapse in the upper indentation. Alternatively, destabilization of the margin above and in the wake of the

trailing flank of the large subducting seamount could have induced the rotational collapse, subsequently triggering the failure of the triangle of lower margin weakened rocks.

Postindentation and postavalanche tectonic processes have also affected the margin. The saw-toothed pattern of the northern wall of the indentation is likely to reflect effects of a postindentation strike-slip tectonic component. Although such effect is difficult to quantify, a cumulative 5-10 km offset can be estimated from our data set. Considering that this motion occurred since 1.5 Ma would imply a strike-slip rate of $0.3\text{--}0.6$ mm yr⁻¹. A 0.17-Myr-old avalanche requires ~ 9 km of shortening to accommodate plate convergence since the slope failure occurred (Figure 15c). Such shortening could have been accommodated by avalanche deposit subduction, internal deformation or thrust motion along its basal plane. Several lines of evidence support limited shortening in the avalanche deposit. Faint west dipping reflectors on seismic line 3033-37 (Figure 9c) are tentatively interpreted as incipient thrusts in the avalanche incoherent mass. These faults may be part of a deformation zone associated with recent motion along the interplate décollement (Figures 5 and 14). Structural

lineaments trending N125°E and N60°E across the avalanche deposit form a pattern of conjugate faults, which is compatible with shortening in response to the N277°E oriented PAC-KER convergence vector (Figure 5). Shortening is also evident within the debris flow. The western part of the debris flow is involved in an incipient accretionary lobe that develops against the toe of the margin (Figure 13). An estimated 3.2 km minimum shortening at this site suggests a 60 ka age for the debris flow. However, this presupposes that the debris flow originally touched the base of the margin at that point and must therefore be regarded as a minimum age.

7.6. Dynamics of Avalanching

7.6.1. Main avalanche: main and secondary lobes. The two lobes of the avalanche are of similar ages since the cover beds of their small, enclosed basins have similar thickness. The splitting of a single avalanche in two lobes may have been controlled by the NW trending high in basement topography that outcrops just seaward of the division between the lobes (R2 in Figure 5). We infer that the main avalanche began in the southern part of the indentation. Its northern edge flowed landward of the basement high. Its main part was diverted south of the high and out across the Hikurangi Trough.

7.6.2. Large frontal blocks. The main Ruatoria avalanche deposit has the largest blocks at its leading edge, unlike most other large avalanche deposits, which have the biggest blocks somewhere in the middle [Jacobs, 1995; Masson, 1996; Moore et al., 1989]. This may be at least partly a function of the original, prefailure profile of the margin as well as relative velocities during transport. If the largest blocks form where the failing mass was thickest, then the oversteepened, tectonically eroded, lower slope of the northern Hikurangi margin would produce the largest blocks near its leading edge. More typical, concave upward slopes might produce them in the middle. In some situations, large blocks can "ground" like icebergs with the rest of the flow moving more quickly around them [Masson et al., 1998]. They can also have the momentum to outrun the rest of an avalanche by trapping fluid or hydroplaning over a fluid substrate at their leading edge [Lipman et al., 1988; Mohrig et al., 1998]. The Ruatoria Knoll and its adjacent blocks moved for over 40 km over a flat plain by riding over thin, soft, unconsolidated, sandy mud turbidites that rest on Cainozoic pelagic drape. The momentum to achieve this came from their initial fall height. If, as we suspect, the initial massive block originated from the lowermost of two large scallops in the southern wall, then the depth difference between the knoll summit and the upper headwall (Figure 8) is ~1000 m, suggesting that the block, which may have been as large as 20 * 35 km, fell by about this height, probably producing a large tsunami. The Ruatoria Knoll is certainly enormous to have moved so far across a flat plain. Its volume is estimated to be ~200 km³. Although large, this is less than a quarter of the size of the basaltic Tuscaloosa Seamount in the Nuanu debris avalanche deposit off Hawaii [Jacobs, 1995]. However, the Ruatoria Knoll may be the largest sedimentary avalanche block so far discovered.

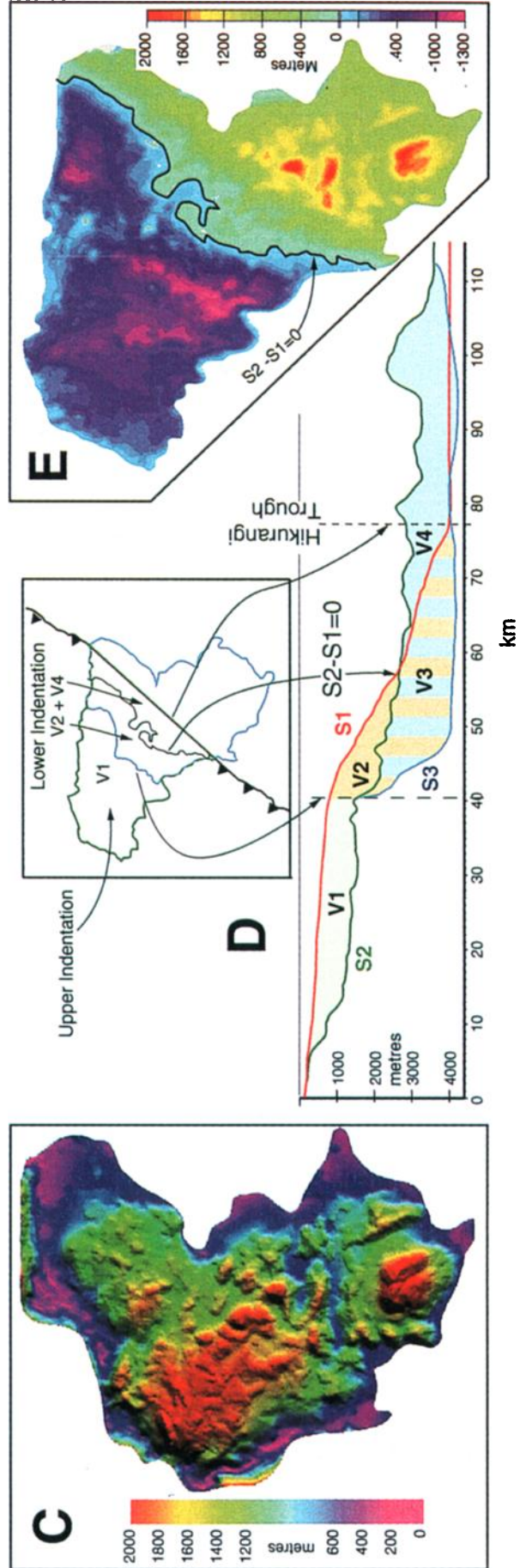
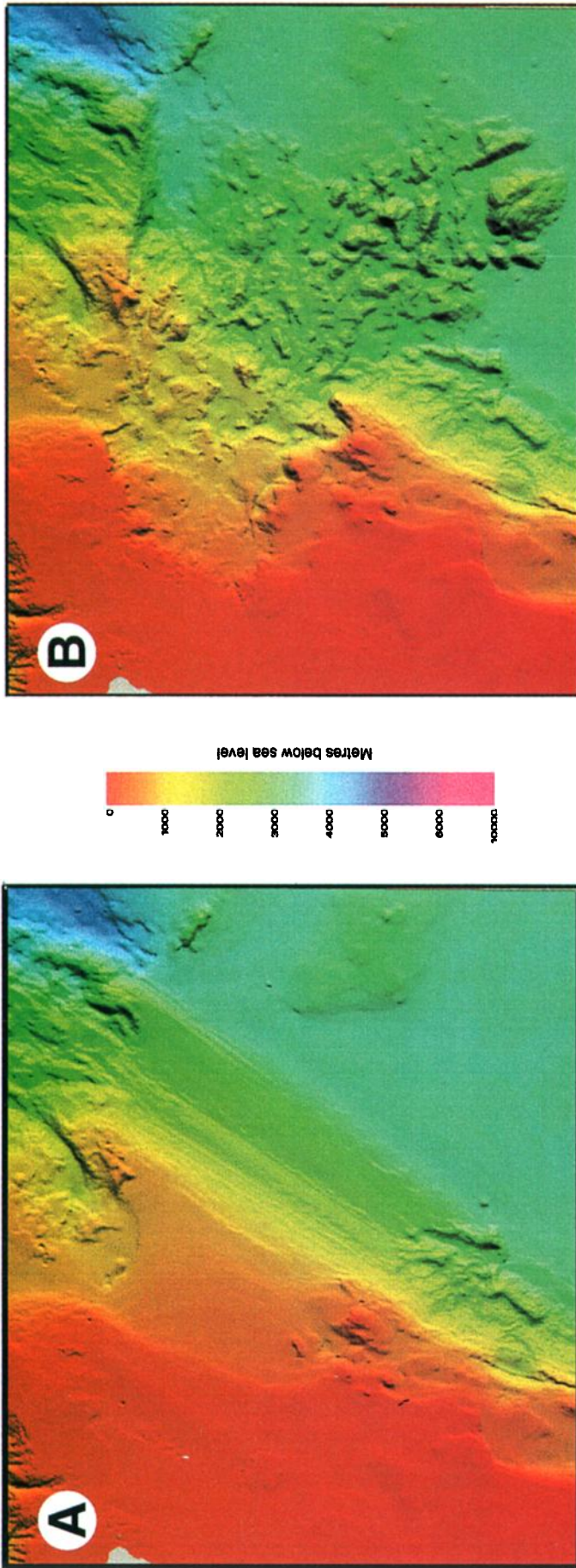
7.6.3. Large avalanche, high-speed, long run out. The main lobe of the avalanche traveled on a 30-km-wide front out across the soft, flat sediments of the Hikurangi Trough. If the avalanche occurred at least 170 kyr ago, then it traveled at least 50 km across the trench because convergence has subsequently carried it ~9 km back toward the margin and

deposition has buried the leading edge. The leading edge of the debris flow associated with the avalanche reached 110 km from the slope. Such run-out distances are dramatic but probably normal in the submarine environment. The Nuanu debris avalanche, off Hawaii, traveled 170 km from the base of the slope, including 50 km across the flat floor of the Hawaii Deep and then for a further 120 km up a slope that rises ~300 m [Jacobs, 1995]. Blocks several kilometers in diameter within the Nuanu avalanche have traveled over 100 km from the foot of slope, while the enormous Tuscaloosa block is >50 km from the slope. The Storrega Slide, off Norway, has a total run-out distance, including distal debris flows, of 800 km [Bugge et al., 1987; Jansen, 1987]; sediment slabs up to 30 km across having slid 200 km down a slope of only 0.3°. There are now many examples of submarine debris deposits that have such extraordinarily long run-out distances [Gee et al., 1999]. Theoretical considerations imply that effective friction decreases with increasing size, so that the enormous debris avalanches and debris flows that occur offshore have long run-out distances [Campbell and Grantmackie, 1995]. Inevitably too, submarine flows are fully saturated, and high excess pore pressure is important, not just at failure, but during the whole event [Norem et al., 1990]. In many cases, this is achieved by an avalanche or debris flow overrunning and incorporating saturated fine sediments from the floor of the avalanche pathway into the basal layer [Gee et al., 1999; Sassa, 1988]. The long run-outs also imply that they have considerable momentum and hence velocity. Onshore debris avalanches have been clocked at 35 m s⁻¹ [Jacobs, 1995], and although offshore avalanches may be slower, they are still likely to be catastrophic events. Although there may have been low friction transport for much of the long run-out, a narrow zone of deformed trough sediments in front of the Ruatoria avalanche deposit suggests high friction "bulldozing," presumably as the avalanche came to a halt.

7.6.4. Debris flow and pressured turbidites. Unlike debris avalanches, debris flows are mainly composed of unconsolidated sediment without mega blocks [Urgeles et al., 1997]. Only a small amount of soft sediment is likely to have come from the failed margin, which consists of tectonically eroded, mid-Cainozoic rocks at or near the seabed. However, the blocky avalanche advancing at high speed for 50 km on a 30-km-wide front may have generated a pressure wave capable of mobilising soft sediment in front of itself. The instability caused by an advancing debris avalanche is known to have triggered a massive debris flow in the Canary Islands [Masson, 1996]. Elsewhere, a more fluid basal phase continues as the main body "freezes" [Gee et al., 1999]. We do not know what thickness of trough sediment was remobilised by the advancing avalanche, but the absence of units T and X (Figure 12) beneath the avalanche mass suggests that it could reach locally 400 m and be 250 m on average over the whole of the trough affected by the avalanche. We suggest that the debris flow is predominantly redeposited trough turbidites, and because of this, its volume is irrelevant in later comparisons of slope failure and indentation volumes.

7.7. Areas, Volumes, and Mass Balance Calculation

Areas and volumes of rocks associated with the Ruatoria indentation, avalanche, and debris flow were calculated using digital terrain models (DTM) compiled from swath bathymetric



and seismic reflection data. In addition to the areas of the indentation, avalanche, and debris flow deposits (Plate 1d and Table 3), three 3-D surfaces were defined and used to calculate volumes. The three surfaces are (S1) the simplified reconstructed topography of the margin and trench, interpreted as before subsidence and avalanche occurred (Plates 1a and 1d), (S2) the present seafloor topography (Plates 1b and 1d), and (S3) the base of the debris avalanche derived from seismic reflection data.

A 3146 km³ gross volume for the debris avalanche (V_a in Table 3; Plate 1c) was calculated by subtracting the base of the avalanche (S3) from the present topography (S2). The volume's accuracy depends on errors made on parameters that include seismic velocities, seismic reflection picking, area contours, and reconstruction of preavalanche topography. Error calculation was simplified by assuming that the debris avalanche is a 62-km-long, 39-km-wide, and 1.3-km-high parallel-sided block on which uncertainties of ± 1 km are estimated for length and width and ± 0.2 km for height. Uncertainties are derived from seismic picking time and velocity. Taking into account these errors yields a ± 629 km³ uncertainty on the avalanche gross volume ($\sim 20\%$). By applying the same 20% error, a 1508 ± 302 km³ gross volume was obtained for the indentation (V_1+V_2 in Plates 1d and 1e and Table 3) by subtracting the present topography (S2) from the reconstructed preindentation topography (S1). Assuming a seismic velocity of 1.7 km s⁻¹, the debris flow generally thins from ~ 170 m thick near the avalanche deposit to ~ 65 m at its abrupt seaward edge, so that, with an area of 8000 km², the debris flow still involves ~ 960 km³ of uncompacted sediment (V_d in Table 3).

Because of its size and comprehensive data set the Ruatoria indentation and associated catastrophic failure appear to be a good natural example to conduct a comparison between the negative volume of the indentation and the positive volumes of the avalanche and debris flow. Because the avalanche, debris flow, and margin rocks have different porosities, a valid comparison must take into account proper compaction factors for each component of the system. In a closed system, such as a passive margin, mass conservation would imply equality between compacted volumes of the missing margin rocks and those of the avalanche and debris flow. The mass conservation equation is:

$$(V_1+V_2+V_3) * C_1 = V_a * C_2 + V_d * C_3 \quad (1)$$

with V_1 , V_2 , and V_3 the volumes of the different parts of the indentation, V_a and V_d the avalanche and debris flow gross

Table 4. Compaction of Avalanche^a

Slices, m	Vol, km ³	P1, %	P2, %	Pav, %	C2, %	Vcomp, km ³
0-300	1208	26	60	46	54	652
300-600	968	22	48	37	63	609
600-900	595	20	38	30	70	416
900-1200	265	19	30	25	75	198
1200-1500	95	18	27	23	77	72
1500-1800	15	17	25	22	78	11
>1800	0.6	15	22	19	81	0.5
Total	3146			37.8	62.2	1958

^aAvalanche deposit is divided into 300-m-thick slices. Slice volumes (Vol) are calculated using GMT 3.1 package. P1 is porosity for rafted blocks; rafted blocks are likely to be fractured and their porosity is considered to be $\sim 20\%$ on average, slightly higher than the margin rocks from which they originated. P2 is porosity for matrix material; avalanche matrix has a depth-dependent porosity similar to that of debris flows drilled elsewhere in the world. Porosities as high as 65% were measured over the upper 100 m below seafloor (bsf) of cores from a debris flow offshore Baja California, and a 60% average porosity is reported over 300 m of cores collected in mass flows at the innerwall of the middle America trench [Baltuck et al., 1985]. We used a 40% porosity at a depth of 600 mbsf, similar to that obtained in silt turbidites at the toe of the Nankai accretionary wedge [Taira et al., 1991]. Porosity per avalanche slice calculated for 40% rafted blocks and 60% matrix: $Pav=0.4*P1+0.6*P2$. Slice compaction is $C2 = 100-Pav$. Compacted volume for each slice is $Vcomp=Vol*C2$. Numbers are rounded up to closest integer except for vol >1800 to nearest decimal.

volumes (Plate 1d and Table 3), and C_1 , C_2 , and C_3 the compaction factors for margin rocks, avalanche, and debris flow deposits, respectively. Volume V_3 appears in both equation members but with different compaction factors since it involves margin rocks which remained in the margin after slope failure. By considering that most of the debris flow consists of remobilized trough fill as discussed above, this equation can be simplified as:

$$(V_1+V_2+V_3) * C_1 - V_a * C_2 = 0. \quad (2)$$

Porosity and therefore compaction estimates in the avalanche deposit and indentation rocks are difficult. Using an average 15% porosity P1 from adjacent East Cape rocks [Field et al., 1997] that we believe are similar in lithology and age to the rocks of the indentation, we derived a compacted $V_1+V_2+V_3$ indentation volume of 2570 km³ (Table 3). On the basis of porosity values indicated in Table 4 and considering that the Ruatoria avalanche deposit was emplaced as a single event, we calculated the porosity of the debris avalanche as a

Plate 1. Models used in mass balance calculations (equal-area Lambert projection). (a) Reconstructed topography of the margin and trench before subsidence and avalanche, (b) present seafloor topography, (c) isopach of the avalanche (S2-S3); (d) cross sections before (S1) and after (S2) subsidence and avalanching; base of avalanche (S3); avalanche ($V_a=S2-S3$) is blue and striped blue areas; V_1 is negative part of (S2-S1) minus V_2 ; V_2 is negative part of (S2-S1) in avalanche contour; V_3 is (S2-S3) in indentation minus V_4 ; V_4 is positive part of (S2-S1) in indentation contour, only used to calculate V_3 ; inset map showing extent of indentation (green) and avalanche (blue), with black line showing no change in height before and after the avalanche ($S2-S1=0$); (e) is the difference in height between topographies after (Plate 1b) and before (Plate 1a) subsidence and avalanching. S1 (stage A) was constructed by replacing indentation topography by interpolated bathymetric contours between indentation's southern and northern walls and by removing avalanche and debris flow on downgoing plate. S3 was obtained by picking avalanche's base on seismic reflection profiles (Figure 2) and converting time to depth using a mean velocity of 2000 m s⁻¹. This value is consistent with that of a debris avalanche volumetrically composed of 40% of rafted blocks and 60% of matrix as estimated from interpretation of strike and dip seismic reflection profiles. Multichannel seismic reflection data on the continental shelf provide a 2400 m s⁻¹ average interval velocity for stratified sediments from which rafted blocks are likely derived. An average value of 1700 m s⁻¹ is assumed for the matrix by comparison with values measured for debris flows [Curry et al., 1982; Moore et al., 1982; von Huene et al., 1985] or sandy, silty trench turbidites [Taira et al., 1991].

weighted average of the matrix porosity and rafted margin blocks for a series of 300-m-thick avalanche slices and derived a corresponding compacted volume for each slice (Table 4). The compacted volume for the debris avalanche is $1958 \pm 392 \text{ km}^3$ assuming a 20% error. This volume is 612 km^3 smaller than the $2570 \pm 514 \text{ km}^3$ compacted indentation volume, a value that is significant with respect to the error on the compacted volumes. In an open system such as the Hikurangi subduction zone a significant negative difference between the compacted indentation and avalanche volumes can be interpreted as the result of avalanche subduction or tectonic erosion of the margin. The lack of evidence of avalanche deposit underthrusting the margin favors tectonic erosion prior to avalanching, a process that is already suggested by the structural analysis of the indentation. One can note that this difference in volumes is close to the 790 km^3 of the compacted upper indentation volume (V1, Plate 1) and consistent with removal of margin material by basal erosion. Our calculations also indicate that the compacted avalanche volume (1958 km^3) match, within errors, the V2+V3 lower indentation volume (1780 km^3). However, if our scenario is correct, then the northern part of the lower slope had already been removed by seamount subduction resulting in the deep-water reentrant (Figure 15b). Therefore, in addition to the triangle the collapse may also have involved fractured rocks from the southern side of the groove-like indentation. This may indicate an originally diffuse southern wall produced by a seamount with a long southeastern "tail" like the nearby Gisborne and Mahia seamounts.

7.8. Scarcity of Avalanches on Active Margins: Making Olistostromes

Compared with the 26 km^3 [Crandell et al., 1984; Hancox and Perrin, 1994] and 50 km^3 [Philip and Ritz, 1999] of the largest onshore landslides and paleolandslides, the $3146 \pm 629 \text{ km}^3$ Ruatoria avalanche deposit is enormous. Even so, it is smaller than landslides reported from passive margins [Bugge et al., 1987; Dingle, 1977], oceanic volcanoes [Moore and Normark, 1994] and collision zones where volumes up to several $10,000 \text{ km}^3$ in multiple events have been reported [Torelli et al., 1997]. On active margins, slope failure behind subducting seamounts is generally comparatively minor [Collot and Fisher, 1989; Pautot and al., 1987; von Huene and Lallemand, 1990]. However, moderately large blocky avalanche deposits have been reported from the Sunda Arc [Moore et al., 1976] and Peruvian margin ($\sim 250 \text{ km}^3$) [Duperret et al., 1995], and landslides comparable in size to the Ruatoria avalanche occur on the southern Oregon Cascadia margin [Goldfinger et al., 2000]. The latter examples occur on an accretionary margin that is subject to subduction erosion and oblique convergence, so that some of the factors causing instability are comparable with those at the Ruatoria indentation. Despite the factors that lead to instability on subduction margins in addition to those on passive margins, large slope failures are comparatively rare. The combination of oblique subduction and regional instability that occur on the northern Hikurangi margin may not be common. However, the main reason may not be infrequent occurrence but rather that slope failure deposits are soon destroyed by continuing convergence that carries them back to the margin they came from. For instance, an avalanche deposit that extends 50 km

beyond the toe of the slope on the northern Hikurangi margin will take only $\sim 1 \text{ Myr}$ to be carried back to the margin, where it will be either shortened and plastered against the margin or carried beneath it. Such deposits may be the gravitationally redeposited and tectonically deformed "chaos breccias" and olistostromes of future landmasses.

8. Conclusions

The main results of our study are as follows:

1. The Ruatoria debris avalanche deposit covers an area of $\sim 3400 \text{ km}^2$, is up to 2 km thick, and has a gross volume of over 3100 km^3 . It has two lobes, the main one originally extending over 50 km from the toe of the margin. It has at least 100 blocks $>1 \text{ km}$ across, including Ruatoria Knoll that is 18 km in maximum dimension. The largest blocks, which may be over 2 km thick, are near its leading edge.

2. Seaward of the avalanche, a 65-170 m thick debris flow deposit that extends over 100 km from the margin, may have formed largely from soft trough sediments mobilized by the pressure wave in front of the avalanche.

3. The Ruatoria debris avalanche and its associated debris flow occurred catastrophically $\sim 170 \pm 40 \text{ ka}$, after failure of a nonaccretionary margin, already weakened by local geologic processes and by fracturing associated with subduction of a large seamount. A major rotational collapse occurred at about the same time in the margin's upper indentation.

4. The avalanche was so large because oblique seamount subduction produced a groove-like indentation obliquely across the margin, leaving a triangle of unstable margin in the acute angle with the deformation front. It was failure of the triangle that produced most of the avalanche.

5. The Ruatoria indentation extends 65 km landward from the toe of the slope to within 25 km from the adjacent land and encloses an area of 3300 km^2 .

6. The Ruatoria indentation has two parts with different ages. The northern strip, with its northern wall approximating the direction of plate convergence, is the remnant of the groove cut obliquely from $\sim 2 \text{ Ma}$ to 0.16 Ma by the subducting seamount. The southern triangle of the indentation and its scalloped southern wall formed the avalanche's headwall at $\sim 0.17 \text{ Ma}$.

7. Volume calculations suggest that the compacted volume of the avalanche deposit is 612 km^3 smaller than that of the indentation, indicating a loss of margin material other than by avalanching and supporting the suggestion that the indentation is primarily a seamount impact depression.

8. The Ruatoria avalanche and debris flow deposits have been carried back toward the margin in the last 170 kyr with indications of compressive deformation in both deposits. The resultant tectonically deformed debris deposits may be a modern analogue of olistostromes in fold belts around the world.

Acknowledgments. We are grateful to the New Zealand Foundation for Research Science and Technology (FRST), the National Institute of Water and Atmospheric Research (NIWA), l'Institut de Recherche pour le Développement (IRD), and the French Ministry of Foreign Affairs for funding and to IFREMER for providing ship time, equipment and software to process data. We thank R. Garlick for help in volume calculations, P. Barnes and A. Kopf for discussions, and G. McMurtry and M. Crozier for helpful suggestions. This is UMR 6526 Géosciences Azur contribution 348.

References

- Abbate, E., V. Bortolotti, and P. Passerini, Olistostromes and olistoliths, *Sediment. Geol.*, **4**, 521 - 557, 1970.
- Anderson, H., E. Smith, and R. Robinson, Normal faulting in a back arc basin: Seismological characteristics of the March 2, 1987, Edgcombe, New Zealand, earthquake, *J. Geophys. Res.*, **95**, 4709-4723, 1990.
- Ballance, P.F., and K.B. Sporli, Northland Allochthon, *J. R. Soc. N.Z.*, **9**, 259-275, 1979.
- Baltuck, M., E. Taylor and K. McDougall, Mass movement along the inner wall of the Middle America Trench, Costa Rica., *Initial Rep. Deep Sea Drill. Proj.*, **84**, 551-565, 1985.
- Barckhausen, U., H. A. Roeser, and R. von Huene, Magnetic signature of upper plate structures and subducting seamounts at the convergent margin off Costa Rica, *J. Geophys. Res.*, **103**, 7079-7093, 1998.
- Barnes, P.M., and B. Mercier de Lépinay, Rates and mechanics of rapid frontal accretion along the very obliquely convergent southern Hikurangi margin, New Zealand, *J. Geophys. Res.*, **102**, 24,931-24,952, 1997.
- Bondevik, S., J.I. Svendsen, and J. Mangerud, Tsunami sedimentary facies deposited by the Storegga tsunami in shallow marine basins and coastal lakes, western Norway, *Sedimentology*, **44**, 1115-1131, 1997.
- Bourgeois, J., Y. Lagabrielle, P. De Wever, E. Suess, and the Nautiper Team, Tectonic history of the northern Peru convergent margin during the past 400 ka, *Geology*, **21**, 531-534, 1993.
- Bradley, J., Megabreccias, in *Synthral Tectonics and Diagenesis*, edited by S.W. Carey, pp. K1-K5, Univ. of Tasmania, Hobart, 1964.
- Bugge, T., S. Befring, R.H. Belderson, T. Eidvin, E. Jansen, N.H. Kenyon, H. Holtedahl, and H.P. Sejrup, A giant three-stage submarine slide off Norway, *Geo Mar. Lett.*, **7**, 191-198, 1987.
- Cadet, J.P., et al., The Japan trench and its juncture with the Kurile trench: Cruise results of the Kaiko project, Leg 3, *Earth Planet. Sci. Lett.*, **83**, 267-284, 1987.
- Campbell, H.J., and J.A. Grantmackie, Jurassic Pholadomyidae (Bivalvia) from New Zealand and New Caledonia, *N. Z. J. Geol. Geophys.*, **38**(1), 47-59, 1995.
- Carpenter, G., Coincident sediment slump/clathrate complexes on the U.S. Atlantic continental slope, *Geo Mar. Lett.*, **1**, 29-32, 1981.
- Carter, L., B. Manighetti, M. Elliot, N. Trustram and B. Gomez, Source, sea-level and circulation effects on the sediment flux to the deep ocean over the past 15 ka off eastern New Zealand, *Global Planet. Change*, in press, 2001.
- Cloos, M., Thrust-type subduction-zone earthquakes and seamount asperities: A physical model for seismic rupture, *Geology*, **20**, 601-604, 1992.
- Collot, J.-Y., and B. Davy, Forearc structures and the tectonic regimes at the oblique subduction zone between the Hikurangi Plateau and the southern Kermadec margin, *J. Geophys. Res.*, **103**, 623-650, 1998.
- Collot, J.-Y., and M.A. Fisher, Formation of Forearc basins by collision between seamounts and accretionary wedges: An example from the New Hebrides subduction zone, *Geology*, **17**, 930-933, 1989.
- Collot, J.-Y., S. Lallemand, B. Pelletier, J.-P. Eissen, G. Glaçon, M.A. Fisher, H.G. Greene, J. Boulin, J. Daniel, and M. Monzier, Geology of the d'Entrécasteaux-New Hebrides Arc collision zone: Results from a deep submersible survey, *Tectonophysics*, **212**, 213-241, 1992.
- Collot, J.-Y., et al., From oblique subduction to intra-continental transpression: structures of the southern Kermadec-Hikurangi margin from multibeam bathymetry, side scan sonar and seismic reflection, *Mar. Geophys. Res.*, **18**, 357-381, 1996.
- Coulter, H.W., and R.R. Migliaccio, Effects of the earthquake of March 27, 1964, at Valdez, Alaska, *U.S. Geol. Surv. Prof. Pap.*, **542-C**, 36 pp., 1966.
- Crandell, D.R., C.D. Miller, R.L. Christiansen, H.X. Glicken, and C.G. Newhall, Catastrophic debris avalanche from an ancestral Mount Shasta volcano, California, in *Geology of the Upper Cretaceous Hornibrook Formation, Oregon and California*, edited by T.H. Nilsen, pp. 197-201, Soc. of Econ. Paleontol. and Mineral., Tulsa, Okla., 1984.
- Curry, J.R., et al., Baja California passive margin transect: Sites 474, 475 and 476, *Initial Rep. Deep Sea Drill. Proj.*, **64**, 35-69, 1982.
- Darby, D.J., and C.M. Meertens, Terrestrial and GPS measurements of deformation across the Taupo back-arc and Hikurangi fore arc regions in New Zealand, *J. Geophys. Res.*, **100**, 8221-8232, 1995.
- Davey, F.J., M. Hampton, J. Childs, M.A. Fisher, K.B. Lewis, and J.R. Pettinga, Structure of a growing accretionary prism, Hikurangi margin, New Zealand, *Geology*, **14**, 663-666, 1986.
- Davey, F.J., S. Henry, and E. Lodolo, A seismic crustal section across the East Cape convergent margin, New Zealand, *Tectonophysics*, **269**, 199-217, 1997.
- Davy, B.W., The influence of subducting plate buoyancy on subduction of the Hikurangi-Chatham Plateau beneath North Island, New Zealand, in *Geology and Geophysics of Continental Margins*, edited by J.S. Watkins, F. Zhiqiang, and K.J. McMillen, pp. 75-91, Am. Assoc. of Petr. Geol., Tulsa, Okla., 1992.
- De Mets, C., R.G. Gordon, D.F. Argus, and S. Stein, Effect of recent revisions to the geomagnetic reversal time scale on estimates of current plate motions, *Geophys. Res. Lett.*, **21**, 2191-2194, 1994.
- Dingle, R.V., The anatomy of a large submarine slump on a sheared continental margin (SE Africa), *J. Geol. Soc. London*, **134**, 293-310, 1977.
- Dingle, R.V., Large allochthonous sediment masses and their role in the construction of the continental slope and rise off southwestern Africa, *Mar. Geol.*, **37**, 333-354, 1980.
- Dominguez, S., S. Lallemand, J. Malavieille, and R. von Huene, Upper plate deformation associated with seamount subduction, *Tectonophysics*, **293**, 207-224, 1998.
- Dominguez, S., J. Malavieille, and S. Lallemand, Deformation of margins in response to seamount subduction insights from sandbox experiments, *Tectonics*, **19**, 182-196, 2000.
- Duperret, A., J. Bourgeois, Y. Labagrielle, and E. Suess, Slope instabilities at an active continental margin: Large-scale polyphase submarine slides along the northern Peruvian margin, between 5°S and 6°S, *Mar. Geol.*, **122**, 303-328, 1995.
- Enos, P., Flow regimes in debris flow, *Sedimentology*, **24**, 133-142, 1977.
- Field, B.D., et al., *Cretaceous-Cenozoic Geology and Petroleum Systems of the East Coast Region, New Zealand, Geol. Monogr.*, **19**, 301 pp., Inst. of Geol. and Nucl. Sci., Lower Hutt, New Zealand, 1997.
- Garcia, M.O., and D.M. Hull, Turbidites from giant Hawaiian landslides: Results from Ocean Drilling Program Site 842, *Geology*, **22**, 159-162, 1994.
- Gee, M.J.R., D.G. Masson, A.B. Watts, and P.A. Allen, The Saharan debris flow: An insight into the mechanics of long runout submarine debris flows, *Sedimentology*, **46**, 317-335, 1999.
- Goldfinger, C., L.D. Kulm, L.C. McNeill, and P. Watts, Super-scale failure of the southern Oregon Cascadia margin, *Pure Appl. Geophys.*, **157**, 1189-1226, 2000.
- Hampton, M.A., H.J. Lee, and J. Locat, Submarine Landslides, *Rev. Geophys.*, **34**, 33-59, 1996.
- Hancox, G.T., and N.D. Perrin, Green Lake landslide: A very large ancient rock slide in Fiordland, New Zealand, in *Seventh International Congress International Association of Engineering Geology*, edited by R. Oliveira, L.F. Rodrigues, A.G. Coelho, and A.P. Cunha, pp. 1677-1689, A.A. Balkema, Brookfield, Vt., 1994.
- Hayward, B.W., The tempestuous 10 million year life of a double arc and intra-arc basin-New Zealand's Northland Basin in the early Miocene, in *Sedimentary Basins of the World, vol. 2, South Pacific Sedimentary Basins*, edited by P.F. Ballance, pp. 113-142, Elsevier Sci., New York, 1993.
- Hinz, K., Tectonic structure of the convergent Pacific margin offshore Costa Rica from multichannel seismic reflection data, *Tectonics*, **15**, 54-66, 1996.
- Holcomb, R.T., and R.C. Searle, Large landslides from oceanic volcanoes, *Mar. Geotechnol.*, **10**, 19-32, 1991.
- Hsu, K.J., Melanges and their distinction from olistostromes, in *Modern and Ancient Geosynclinal Sedimentation, Spec. Publ.*, **19**, edited by R.H. Dott and R.H. Shaver, pp. 321-333, Soc. of Econ. Paleontol. and Mineral., Tulsa, Okla., 1974.
- Jacobs, C.L., Mass-wasting along the Hawaiian Ridge: giant debris avalanches, in *Atlas of Deep Water Environments: Architectural Style in Turbidite Systems*, edited by K.T. Pickering et al., pp. 26-28, Chapman and Hall, New York, 1995.
- Jansen, E., S. Befring, T. Bugge, T. Eidvin, H. Holtedahl and H.P. Sejrup, Large submarine slides on the Norwegian continental margin, sediments, transport and timing, *Mar. Geol.*, **78**, 77-107, 1987.

- Katz, H.R., Probable gas hydrate in continental slope east of the North Island, New Zealand, *J. Pet. Geol.*, 3, 315-324, 1981.
- Katz, H.R., Plate margin transition from oceanic arc-trench to continental system: The Kermadec-New Zealand example, *Tectonophysics*, 87, 49-64, 1982.
- Kear, D., and B.C. Waterhouse, Onehaki chaos-breccia of Northland, *N. Z. J. Geol. Geophys.*, 10, 629-646, 1967.
- Lallemand, S.E., and N. Chamot-Rooke, Sur la cause du décrochement sénestre entre les fosses du Japon et des Kouriles: Subduction-collision d'un ancien volcan sous-marin, *C. R. Acad. Sci.*, 303, 1433-1448, 1986.
- Lallemand, S.E., and X. Le Pichon, Coulomb wedge model applied to subduction of seamounts in the Japan Trench, *Geology*, 15, 1065-1069, 1987.
- Lallemand, S., J.-Y. Collot, B. Pelletier, C. Rangin, and J.-P. Cadet, Impact of oceanic asperities on the tectonogenesis of modern convergent margins, *Oceanol. Acta*, 10, 17-30, 1990.
- Lallemand, S.E., P.S. Schnurle, and J. Malavieille, Coulomb theory applied to accretionary and non accretionary wedges: Possible causes for tectonic erosion and/or frontal accretion, *J. Geophys. Res.*, 99, 12,033-12,055, 1994.
- Lenat, J.-F., P. Vincent, and P. Bachelery, The off-shore continuation of an active basaltic volcano: Piton de la Fournaise (Reunion Island, Indian Ocean); structural and geomorphological interpretation from Sea Beam mapping, *J. Volcanol. Geotherm. Res.*, 36, 1-36, 1989.
- Lerche, I., and E. Bagirov, Guide to gas hydrate stability in various geological settings, *Mar. Pet. Geol.*, 15, 427-437, 1998.
- Lewis, K.B., The 1500-km-long Hikurangi Channel: Trench-axis channel that escapes its trench, crosses a plateau, and feeds a fan drift, *Geo Mar. Lett.*, 14, 19-28, 1994.
- Lewis, K.B., and D.J. Bennett, Structural patterns on the Hikurangi margin: An interpretation of new seismic data, in *New Seismic Profiles, Cores and Dated Rocks From the Hikurangi Margin, New Zealand*, edited by K.B. Lewis, pp. 3-25, N. Z. Oceanogr. Inst., Wellington, 1985.
- Lewis, K.B., and B.A. Marshall, Seep faunas and other indicators of methane-rich dewatering on New Zealand convergent margins, *N. Z. J. Geol. Geophys.*, 39, 181-200, 1996.
- Lewis, K.B., and J.R. Pettinga, The emerging, imbricate frontal wedge of the Hikurangi margin, in *Sedimentary Basins of the World, vol.2, South Pacific Sedimentary Basins*, edited by P.F. Ballance, pp. 225-250, Elsevier Sci., New York, 1993.
- Lewis, S.D., J.W. Ladd, and T.R. Bruns, Structural development of an accretionary prism by thrust and strike-slip faulting: Shumagin region, Aleutian Trench, *Geol. Soc. Am. Bull.*, 100, 767-782, 1988.
- Lewis, K.B., J.-Y. Collot, and S. Lallemand, The dammed Hikurangi Trough: A channel-fed trench blocked by subducting seamounts and their wake avalanches (New Zealand-France GeodyNZ Project), *Basin Res.*, 10, 441-468, 1998.
- Lipman, P.W., W.R. Normark, J.G. Moore, J.B. Wilson, and C.E. Gutmacher, The giant submarine Alika Deris Slide, Mauna Loa, Hawaii, *J. Geophys. Res.*, 93, 4279-4299, 1988.
- Masson, D.G., Catastrophic collapse of the volcanic island of Hierro 15 ka ago and the history of landslides in the Canary Islands, *Geology*, 24, 231-234, 1996.
- Masson, D.G., L.M. Parson, J. Milsom, G. Nichols, N. Sikumbang, B. Dwiyanto, and H. Kallagher, Subduction of seamounts at the Java Trench: A view with long-range sidescan sonar, *Tectonophysics*, 185, 51-65, 1990.
- Masson, D.G., M. Canals, B. Alonso, R. Urgeles, and V. Huhnerbach, The Canary debris flow: Source area morphology and failure mechanisms, *Sedimentology*, 45, 411 - 432, 1998.
- Mazengarb, C. Late Neogene structural development of eastern Raukumara Peninsula: implications for oil exploration, in *New Zealand Petroleum Conference Proceedings*, pp. 201-205, Publicity Unit, Crown Miner., Minist. of Commer., Queenstown, 1998.
- McGlone, M.S., and J.M. Wilmhurst, Dating initial Maori environmental impact in New Zealand, *Quat. Int.*, 59, 5-16, 1999.
- Mohrig, D., K.X. Whipple, M. Hondzo, C. Ellis, and G. Parker, Hydroplaning of subaqueous debris flows, *Geol. Soc. Am. Bull.*, 110, 387-394, 1998.
- Moore, D.G., J.P. Curray, and F.J. Emmel, Large submarine slide (olistostrome) associated with Sunda Arc subduction zone, northeastern Indian Ocean, *Mar. Geol.*, 21, 211-226, 1976.
- Moore, D.G., J.R. Curray and G. Einsele, Salado-Vinorama submarine slide and turbidity current off the southeast tip of Baja California, *Initial Rep. Deep Sea Drill. Proj.*, 64, 1071-1082, 1982.
- Moore, J.G., and G.W. Moore, Deposit from a giant wave on the island of Lanai, Hawaii, *Science*, 226, 1312-1315, 1984.
- Moore, J.G., and W.R. Normark, Giant Hawaiian landslides, *Annu. Rev. Earth Planet. Sci.*, 22, 119-144, 1994.
- Moore, J.G., D.A. Clague, R.T. Holcomb, P.W. Lipman, W.R. Normark, and M.E. Torresan, Prodigious submarine landslides on the Hawaiian Ridge, *J. Geophys. Res.*, 94, 17,465-17,484, 1989.
- Mortimer, N., and D.L. Parkinson, Hikurangi Plateau: A Cretaceous large igneous province in the southwest Pacific Ocean, *J. Geophys. Res.*, 101, 687-696, 1996.
- Mulder, T., and P. Cochonat, Classification of offshore mass movements, *J. Sediment. Res.*, 66, 43-5, 1996.
- Naylor, M.A., Debris flow (olistostromes) and slumping on a distal passive continental margin: the Palombini limestone-shale sequence of the northern Apennines, *Sedimentology*, 28, 113-123, 1981.
- Norem, H., J. Locat, and B. Scheildrop, An approach to the physics and modelling of submarine flowslides, *Mar. Geotechnol.*, 9, 93-111, 1990.
- Orange, D.L., and M.B. Underwood, Patterns of thermal maturity as diagnostic criteria for interpretation of melanges, *Geology*, 23, 1, 144-1,148, 1995.
- Papathodorou, G., T. Hasiotis, and G. Ferentinos, Gas-charged sediments in the Aegean and Ionian Seas, Greece, *Mar. Geol.*, 112, 171-184, 1993.
- Pautot, G., et al., Deep-sea submersible survey in the Sugura, Sagami and Japan trenches: Preliminary results of the 1985 Kaiko cruise, Leg 2, *Earth Planet. Sci. Lett.*, 83, 300-312, 1987.
- Pelletier, B., and R. Louat, Seismotectonics and present-day relative plate motions in the Tonga-Lau and Kermadec-Havre region, *Tectonophysics*, 165, 237-250, 1989.
- Philip, H., and J.-F. Ritz, Gigantic paleolandslide associated with active faulting along the Bogd fault (Gobi-Altay, Mongolia), *Geology*, 27, 211-214, 1999.
- Rait, G.J., Tectonics of the East Coast Allochthon, 164 pp., *Geol. Soc. of N. Z.*, 1995.
- Reyners, M., and P. McGinty, Shallow subduction tectonics in the Raukumara Peninsula, New Zealand, as illuminated by earthquake focal mechanisms, *J. Geophys. Res.*, 104, 3025-3034, 1999.
- Reyners, M., D. Eberhart-Phillips, and G. Stuart, A three-dimensional image of shallow subduction: crustal structure of the Raukumara Peninsula, New Zealand, *Geophys. J. Int.* 137, 873-890, 1999.
- Ridd, M.F., Mud volcanoes in New Zealand, *Am. Assoc. Pet. Geol. Bull.*, 54, 601-616, 1970.
- Sassa, K., Geotechnical model for the motion of landslides, in *Landslides-Glissements de Terrains*, edited by C. Bonnard, pp. 37-55, A. A. Balkema, Brookfield, Vt., 1988.
- Scholz, C.H., and C. Small, The effect of seamount subduction on seismic coupling, *Geology*, 25, 487-490, 1997.
- Smith, E.G.C., T.A. Stern, and M. Reyners, Subduction and back-arc activity at the Hikurangi Convergent Margin, New Zealand, *Pure Appl. Geophys.*, 129, 203-231, 1989.
- Stewart, R.B., and V.E. Neall, Chronology of palaeoclimate change at the end of the last glaciation, *Nature*, 311, 47-48, 1984.
- Stoneley, R., Marl diapirism near Gisborne, New Zealand, *N. Z. J. Geol. Geophys.*, 5, 630-641, 1962.
- Stoneley, R., A lower Tertiary decollement on the east coast, North Island, New Zealand, *N. Z. J. Geol. Geophys.*, 11, 128-156, 1968.
- Strong, C.P., Late cretaceous foraminifera from Hikurangi Plateau, New Zealand, *Mar. Geol.*, 119, 1-5, 1994.
- Taira, A., et al., Site 808, *Proc. Ocean Drill. Program Initial Rep.*, 131, 71-285, 1991.
- Torelli, L., R. Sartori, and N. Zitellini, The giant chaotic body in the Atlantic Ocean off Gibraltar: New results from a deep seismic survey, *Mar. Pet. Geol.*, 14, 125-138, 1997.
- Urgeles, R., M. Canals, J. Baraza, B. Alonso, and D. Masson, The most recent megaslides of the Canary Islands: El Golfo debris avalanche and Canary debris flow, west El Hierro Island, *J. Geophys. Res.*, 102, 20,305-20,323, 1997.
- von Huene, R., and S. Lallemand, Tectonic erosion along the Japan and Peru convergent margins, *Geol. Soc. Am. Bull.*, 102, 704-720, 1990.
- von Huene, R., et al., Site 565, *Initial Rep. Deep Sea Drill. Proj.*, 84, 21-78, 1985.
- von Huene, R., J. Bourgois, J. Miller, and G. Pautot, A large, tsunamogenic landslide and debris flow along the Peru Trench, *J. Geophys. Res.*, 94, 1703-1714, 1989.
- von Huene, R., et al., Morphotectonic features of the Costa Rican Pacific margin surveyed during the Sonne 76 cruise, in *Geologic and*

- Tectonic Development of the Caribbean Plate Boundary in Southern Central America*, edited by P. Mann, Spec. Pap. Geol. Soc. Am., 295, 291-308, 1995.
- von Huene, R., T. Reston, N. Kukowski, G. Dehghani, W. Weinrebe, X. Le Pichon, and S. Lallemand, A subducting seamount beneath the Mediterranean Ridge, *Tectonophysics*, 271, 249-261, 1997.
- Walcott, R.I., Geodetic strains and large earthquakes in the axial tectonic belt of North Island, New Zealand, *J. Geophys. Res.*, 83, 4419-4429, 1978.
- Walcott, R.I., Geodetic strain and the deformation history of the North Island of New Zealand during the late Cainozoic, *Philos. Trans. R. Soc. London, Ser. A*, 321, 163-181, 1987.
- Weaver, P.P.E., Sediment mass wasting in the Canary Basin., in *Atlas of Deep Water Environments: Architectural Style in Turbidite Systems*, edited by K.T. Pickering et al., pp. 289-297, Chapman and Hall, New York, 1995.
- Wood, R., and B. Davy, The Hikurangi Plateau, *Mar. Geol.*, 118, 153-173, 1994.
- Wright, I.C., Pre-spread rifting and heterogeneous volcanism in the southern Havre Through back-arc basin, *Mar. Geol.*, 113, 179-200, 1993.
-
- J.-Y. Collot, UMR Géosciences Azur, IRD, B.P. 48, F-06235 Villefranche sur mer, France. (collot@obs-vlfr.fr)
- S. Lallemand, Laboratoire de Géophysique, Tectonique et Sédimentologie, Université de Montpellier II, F-34000 Montpellier, France. (lallemand@dstu.univ-montp2.fr)
- G. Lamarche and K. Lewis, NIWA, P.O. Box 14901, Wellington, New Zealand. (g.lamarche@niwa.cri.nz; k.lewis@niwa.cri.nz)

(Received April 13, 2000; revised December 8, 2000; accepted December 22, 2000.)